Article

Tests of model predictions for the responses of stellar spectra and absorption-line indices to element abundance variations. Tests of model predictions for the responses of stellar spectra and absorption-line indices to element abundance variations.

Sansom, Anne E

Sansom, Anne E (2013) Tests of model predictions for the responses of stellar spectra and absorption-line indices to element abundance variations. Tests of model predictions for the responses of stellar spectra and absorption-line indices to element abundance variations. MNRAS, 435 (2). pp. 952-974. ISSN 2013MNRAS435.952S

Monthly Notices
of the
ROYAL ASTRONOMICAL SOCIETY

MNRAS **435,** 952–974 (2013)
Advance Access publication 2013 August 29

doi:10.1093/mnras/stt1283

Tests of model predictions for the responses of stellar spectra and absorption-line indices to element abundance variations

A. E. Sansom,[1]★ A. de Castro Milone,[2] A. Vazdekis[3,4] and P. Sánchez-Blázquez[5]

[1]*Jeremiah Horrocks Institute, School of Computing, Engineering and Physical Sciences, University of Central Lancashire, Preston, PR1 2HE*
[2]*Divisão de Astrofísica, Instituto Nacional de Pesquisas Espaciais, Av. dos Astronautas 1758, São José dos Campos, SP 12227-010, Brazil*
[3]*Instituto de Astrofísica de Canarias, C/ Vía Láctea s/n, E-38200 La Laguna, Tenerife, Spain*
[4]*Departamento de Astrofísica, Universidad de La Laguna, E-38205 La Laguna, Tenerife, Spain*
[5]*Departamento de Física Teórica, Universidad Autónoma de Madrid, E-28049, Spain*

Accepted 2013 July 12. Received 2013 July 9; in original form 2012 October 12

ABSTRACT

A method that is widely used to analyse stellar populations in galaxies is to apply the theoretically derived responses of stellar spectra and line indices to element abundance variations, which are hereafter referred to as response functions. These are applied in a differential way, to base models, in order to generate spectra or indices with different abundance patterns. In this paper, sets of such response functions for three different stellar evolutionary stages are tested with new empirical [Mg/Fe] abundance data for the medium-resolution Isaac Newton Telescope library of empirical spectra (MILES). Recent theoretical models and observations are used to investigate the effects of [Fe/H], [Mg/H] and overall [Z/H] on spectra, via ratios of spectra for similar stars. The global effects of changes in abundance patterns are investigated empirically through direct comparisons of similar stars from MILES, highlighting the impact of abundance effects in the blue part of the spectrum, particularly for lower temperature stars. It is found that the relative behaviour of iron-sensitive line indices are generally well predicted by response functions, whereas Balmer line indices are not. Other indices tend to show large scatter about the predicted mean relations. Implications for element abundance and age studies in stellar populations are discussed and ways forward are suggested to improve the match with the behaviour of spectra and line-strength indices observed in real stars.

Key words: techniques: spectroscopic – stars: abundances – stars: atmospheres – galaxies: abundances – galaxies: stellar content.

1 INTRODUCTION

Element abundance patterns in galaxies hold vital clues to the formation and evolution of their stellar populations. Stellar sources of chemical enrichment contribute different abundance distributions on different time-scales. This provides a potential clock for understanding how the integrated stellar population was built up over time, and hence the star formation history of a galaxy. The power of this technique relies on our understanding of the different element abundance contributions, on the quality of the spectroscopic data and on the ability to accurately recover representative element abundances in integrated stellar populations from the available data.

Supernova explosions provide the main sources of chemical enrichments for future generations of stars. Type II supernova (SNII) explosions enrich the interstellar medium (ISM) over a short time-scale ($t \leq 10^8$ yr) with a wide range of heavy elements (including α elements, iron-peak and r-process elements). SNIa explosions enrich the ISM over a much more extended time-scale, with mainly iron-peak elements, including prompt ($t \sim 10^8$ yr) and delayed ($t > 10^8$ to $\sim 10^{10}$ yr) enrichment (Sullivan et al. 2006; Mannucci 2008; Maoz, Sharon & Gal-Yam 2010). Hence, the ratio of α elements to iron is an important indicator of the time-scale of star formation. Intermediate-mass stars contribute to the lighter elements over a relatively long time-scale ($t > 10^8$ to $\sim$few $\times 10^9$ yr). Additional contributions might come from red giant (RG) stars and cosmic ray reactions, but these are not important for the elements considered in the present analysis. The understanding of the relevant element abundance contributions and time-scales is still uncertain in some cases. However, the match of models to the abundance pattern observed in our own Galaxy (Timmes, Woosley & Weaver 1995; Tsujimoto et al. 1995; Kobayashi et al. 2006), within a factor of 2 for most elements up to the iron peak, gives some confidence that these contributions are broadly understood.

Methods of measuring abundance patterns in stellar populations range from colours (e.g. James et al. 2006), which are known to

★E-mail: aesansom@uclan.ac.uk

harbour degeneracies (e.g. Worthey 1994; Carter et al. 2009), to broad and narrow spectral features (e.g. Rose 1994; Worthey 1994; Worthey & Ottaviani 1997, hereafter WO97; Serven, Worthey & Briley 2005; Cenarro et al. 2009). Another, related approach is to use spectral indices from scaled-solar populations to generate proxies for abundance ratios (see fig. 25 of Vazdekis et al. 2010). There have also been efforts to generate fully integrated spectra (e.g. Coelho et al. 2007; Lee et al. 2009a, hereafter L09; Percival et al. 2009) and to use full spectral fitting (e.g. Walcher et al. 2009) for abundance ratio analysis. However, these methods and models are still under development. Information about metallicities, the ratio of α elements to iron and, sometimes, individual element abundances is recovered from spectral features. One widely used method is to apply element abundance response functions derived from theoretical stellar spectra, which quantify the changes in line-strength indices to variations of individual chemical elements. These response functions are built using theoretical model atmospheres, combined with radiative transfer codes and extensive line lists of atomic and molecular features. These are applied in a differential way, to base models from theoretical or observed spectra with standard abundance patterns, in order to generate spectra or indices for different abundance patterns (e.g. Trager et al. 2000; Thomas, Maraston & Bender 2003; Graves & Schiavon 2008; Sansom & Northeast 2008). This can have the advantage of reducing problems associated with absolute line-strength predictions from theory, which are limited by incomplete line and molecular band transition information.

Much of the analysis of galaxy abundance ratios in the literature is based on the Lick spectral indices (with band definitions originally from Worthey 1994; WO97) and response functions for these from theoretical stellar spectra (e.g. Tripicco & Bell 1995, hereafter TB95; Korn, Maraston & Thomas 2005, hereafter K05; Houdashelt et al. 2002, hereafter H02; Tantalo, Chiosi & Piovan 2007, hereafter T07; L09). Differential application of theoretical models, to empirical star or simple stellar population (SSP) indices, is currently thought to be one of the best approaches to explore stellar populations with different abundance patterns (e.g. see the discussion in Walcher et al. 2009).

In particular, the response functions of K05 are widely applied. Here, we give some examples. Mendel, Proctor & Forbes (2007) have used response functions from both K05 and H02 to derive the ages, metallicities and alpha-element abundances in globular clusters. Schiavon (2007) have used response functions from K05, applied differentially to the empirical stellar library of Jones (1999), in order to generate SSP models with different abundance patterns. These SSPs have since been used in several studies to measure the ages and compositions of star clusters and galaxies. Thomas, Johansson & Maraston (2011) have used response functions from K05 to derive the ages and abundances of six elements, in order to investigate the chemical patterns in globular clusters. Annibali et al. (2011) have used response functions from K05 to derive the ages and [α/Fe] ratios of dwarf and giant early-type galaxies.

Examples of the use of other response functions in the literature include the following. Lee, Worthey & Dotter (2009b) have used the α-enhancement dependences found in L09, to study the effects of horizontal branch stars and the initial mass function on the integrated light of globular clusters. Serra et al. (2008) have used the response function from G. Worthey (private communication), based on the work of L09, to study stellar abundance variations as a function of cold and ionized gas content in a sample of field early-type galaxies.

In this paper, we test the robustness of some of the studies listed above that attempt to accurately represent the dependence of spectral line strengths on differing abundance patterns in stars. We do this by testing the response functions, on which the above studies rely, on a star-by-star basis, comparing model predictions to empirical observations of individual stars. This is likely to be one of the cleanest approaches to testing the methods used to measure abundance patterns that are most widely used in the literature. It has the drawback that real star abundance patterns are likely to be more complex than the theoretical models assume; however, it will provide a grounding for the methods used to measure [α/Fe].

New empirical data for stars are now available, which these response functions can be tested against in order to check their accuracy against real stars. These data are from the medium-resolution Isaac Newton Telescope library of empirical spectra (MILES; Sánchez-Blázquez et al. 2006, hereafter SB06; Cenarro et al. 2007). This spectral library consists of 985 stars covering a wide range of parameter space in effective temperature $T_{\rm eff}$, surface gravity g and metal abundance (characterized by [Fe/H][1]). For 752 of these stars, the [Mg/Fe] ratio has been compiled in a catalogue (Milone et al. 2011, hereafter M11). This compilation is based on standardized results from high spectral resolution studies, plus new measurements from MILES, calibrated to a standard scale using high-resolution measurements. In this work, we make use of [Mg/Fe] measurements as a proxy for all [α/Fe] abundance ratios as a homogeneous nucleosynthetic class and we compare differential results from these empirical data with corresponding differential predictions from theoretical models.

This paper is set out as follows. In Section 2, we give an overview of the current knowledge of the effects of differing abundance patterns in stars on their spectral features, and we discuss the published response functions and empirical data used in this paper. In Section 3, we apply the response functions and compare them with empirical data. In Section 4, we compare the effects on spectra resulting from differing abundance patterns for the theoretical and empirical spectra of stars. We discuss the results in Section 5 and we conclude in Section 6.

2 EFFECTS OF ABUNDANCE PATTERNS

2.1 General considerations

The chemical and physical conditions of a stellar photosphere are imprinted on its emergent spectrum. The major parameter that defines the overall shape of a photospheric spectrum is the effective temperature. Then, the abundance pattern, surface convection and surface gravity also affect its spectrum. In particular, we are interested in how the photospheric element abundance pattern affects its emergent spectrum. The overall metallicity [Z/H] can affect the continuum shape as well as absorption-line strengths. Iron is the main element that is analysed in most spectroscopic studies of stars (especially FGK types) to quantify the chemical abundance in a photosphere. This is because of the existence of a myriad of Fe I and Fe II lines in the optical range, which are measurable at high resolution and which contribute to spectral line strengths or narrow-band indices at lower resolution. The effects of other elements can sometimes be more isolated to particular spectral features. However, to accurately measure these effects, it is very important to be clear about what is meant by the metallicity of the star ([Z/H] or [Fe/H]). This is true both for the observations and for the theoretical models used to investigate them.

[1] $[{\rm X/H}] = \log[n({\rm X})/n({\rm H})]_{\rm star} - \log[n({\rm X})/n({\rm H})]_{\rm sun}$, where $n({\rm X})/n({\rm H})$ is the number abundance ratio of element X, such as Fe, relative to hydrogen.

A simplification assumed in recent years, in order to probe beyond overall metallicity and to uncover the information available in abundance ratios for galaxies, is that all the α elements behave in lock-step. This is a reasonable approximation based on the observational evidence for some α elements from stars in our Galaxy. However, it is not exactly correct (e.g. Bensby et al. 2005; Neves et al. 2009; Franchini et al. 2011). In addition, when handling the metallicity budget in stars, oxygen and carbon are important contributors. Their patterns do not follow the α elements, iron-peak elements or global metallicity, but have their own significant contributions (e.g. McWilliam et al. 2008). For this reason, it is more directly linked to observations if models predict the behaviour of varying abundance patterns at fixed [Fe/H] (i.e. a single important element) rather than at fixed [Z/H], which is more open to interpretation. Unfortunately, this is not always the case, and to recover changes at fixed [Fe/H] from these models, it is necessary to make assumptions about how [Z/H], [Fe/H] and other abundance indicators, such as [α/Fe], are related. These uncertainties have been more widely discussed in the literature in recent years (e.g. Schiavon 2007) and are emphasized here to clarify the difficulties in accurately determining abundance patterns from observed stars or stellar populations, given the currently available models.

2.2 Response functions in the literature

Response functions tabulate how much various spectral line strengths alter with element abundance changes in the theoretical model spectra. The application of these response functions makes it possible for empirical or theoretical line strengths to be modified for particular abundance patterns, notably enhanced [α/Fe] ratios, compared to that of local solar neighbourhood stars. Particular response functions in the literature are as follows.

(i) TB95 have provided models for three stars: a cool dwarf (CD), a turn-off (TO) and a RG star on a 5-Gyr isochrone. Response functions have shown how the Lick indices varied because of a factor of 2 increase in individual elements and in overall metallicity (i.e. from [X/H] = 0.0 to [X/H] = +0.3).

(ii) H02 (similar to TB95, but with updated spectral line lists) have added Hγ and Hδ indices and carbon enhancements reduced to +0.15, rather than +0.3 as used for other elements varied in their study (see Worthey 2004, section 3.3). This latter change was an attempt to prevent the C_2 swan bands from becoming unrealistically strong in carbon-rich stars. Their response functions for three stars can be obtained from http://astro.wsu.edu/hclee/HTWB02.

(iii) K05 (similar to TB95, but for a wider range of initial metallicities and star types) have provided response functions again tabulated for a factor of 2 increase in element abundances from the base models.

(iv) T07 have generated response functions for a change of α elements from [α/H] = 0.0 (i.e. solar) to [α/H] = +0.4. Individual elements are not varied, but α elements are enhanced as a group. They start from base stars that cover a wider range of atmospheric parameters than in TB95, covering up to five values of $T_{\rm eff}$ and four values of $\log g$. T07 do not give responses for overall changes in metallicity. These response functions have not yet been widely used subsequently in the literature.

(v) L09 have expanded the work of H02 and generated response functions for SSPs using many (∼35) theoretical star spectra at solar metallicity times 10 individual element enhancements (at fixed overall metallicity). Their theoretical spectra are binned to 0.5 Å per flux point (however, their response functions are not very sensitive to spectral resolution). Plots of some comparisons with K05 for individual theoretical stars are given at http://astro.wsu.edu/hclee/NSSPM_II_Lick.html; these show similar, but not identical, responses in general between K05 and their evaluations.

Some of the above response functions varied the amounts of individual elements present in the atmospheres; however, they did not always track changes in opacity self-consistently. For example, K05 tracked opacity changes for overall metallicity changes ([Z/H]), but treated individual elements like trace elements, whereas the theoretical spectra of L09 were consistently calculated for each abundance pattern. More recent theoretical spectra are available, which take into account non-solar abundance patterns plus a more self-consistent approach (e.g. Coelho et al. 2005; Munari et al. 2005). In particular, the theoretical stellar spectra of Coelho et al. (2005) are compared to observational spectra in Section 4 of this paper. Response functions for Lick indices are not generally available for these recent theoretical stellar libraries.

Table 1 shows the basic characteristics, assumptions and tools used in the generation of published element response functions for stars. This shows the range of different models and assumptions used in generating these response functions.

2.3 Observations: MILES Lick line-strength indices

For the 752 stars for which [Mg/Fe] could be obtained in M11, we have measured the line-strength indices in the Lick/IDS system (with the definitions of Trager et al. 1998 and WO97) in the latest version of the MILES stellar spectra (Falcón-Barroso et al. 2011). Errors were estimated from uncertainties caused by photon noise and wavelength calibration (errors in the flux calibration were not

Table 1. This table shows the basic assumptions and tools used in the generation of published element response functions for stars. The elements listed are those tabulated in the response functions. See the references in the first column for details of other references and names given in this table.

Reference	Stellar atmosphere code	Spectral synthesis code	Other comments	α elements	Other elements
H02	MARCS	SSG (Bell & Gustafsson 1989)	Updated TB95	O, Mg, Si, Ca, Ti	C, N, Na, Cr, Fe
K05	MAFAGS	LINFOR	Excludes TiO	O, Mg, Si, Ca, Ti	C, N, Na, Cr, Fe
T07	ATLAS9	Munari et al. (2005)	Combined α	α-enhancement	[Z/Z$_\odot$]
L09	PLEZ	FANTOM (Coelho et al. 2005)	Coolest stars	O, Ne, Mg, Si, S, Ca, Ti	C, N, Fe
L09	ATLAS	FANTOM (Coelho et al. 2005)	Cool stars		
L09	MARCS	SSG (Bell, Paltoglou & Tripicco 1994)	Medium $T_{\rm eff}$		
L09	ATLAS	SYNTHE (Kurucz 1970)	Hot stars		

Table 2. Lick resolution and MILES average errors. The first column gives the index name; the second column gives the final spectral resolution (FWHM) at which each index was measured; the third column gives the average Lick index errors for the MILES stellar data base and their units are given in the last column.

Index	Resolution (Å)	Average index error	Index units
$H\delta_A$	10.9	0.1895	Å
$H\delta_F$	10.9	0.1278	Å
CN_1	10.6	0.0050	mag
CN_2	10.6	0.0061	mag
Ca4227	10.1	0.0850	Å
G4300	9.8	0.1427	Å
$H\gamma_A$	9.5	0.1533	Å
$H\gamma_F$	9.5	0.0912	Å
Fe4383	9.2	0.1921	Å
Ca4455	9.1	0.0970	Å
Fe4531	9.0	0.1377	Å
C_24668	8.8	0.1942	Å
$H\beta$	8.4	0.0740	Å
Fe5015	8.4	0.1528	Å
Mg_1	8.4	0.0016	mag
Mg_2	8.4	0.0018	mag
Mgb	8.4	0.0653	Å
Fe5270	8.4	0.0692	Å
Fe5335	8.4	0.0698	Å
Fe5406	8.4	0.0505	Å
Fe5709	9.2	0.0890	Å
Fe5782	9.2	0.0849	Å
NaD	9.5	0.1103	Å
TiO_1	9.7	0.0026	mag
TiO_2	9.7	0.0023	mag

taken into account, but the relative flux calibration in the MILES stars have been proved to be very accurate). The line-strength indices were transformed to the Lick system taking into account differences in spectral resolution between the Lick/IDS system and MILES stars, following the prescriptions in WO97 (see their table 8). Table 2 gives the final resolution at which each index was measured. No further offsets were applied to the measured indices, because both the theoretical response functions and the MILES observations were not converted to the Lick/IDS flux system (see K05, section 2.4). Average errors and units for each index are given in the last two columns in Table 2. Appendix A lists all the parameters and Lick indices for MILES stars used in Figs 1 and 2 of this paper.

3 TESTING RESPONSE FUNCTIONS

The original study of TB95 opened the way to differential techniques for tracking abundance ratios. Their work was followed by the more comprehensive study of K05, who included the same theoretical base, solar metallicity stars as TB95, but also explored response functions from lower and higher metallicity base stars. K05 have shown that their work agrees well with the results of TB95 and they have also added results for $H\gamma$ and $H\delta$ indices. Response functions from both studies have been widely applied in the literature. However, we do not test the TB95 response functions here because those of K05 and H02 can be considered as expansions of that earlier work. Theoretical spectra from H02 were revised and expanded by L09 to form SSPs and their theoretical spectra and SSP

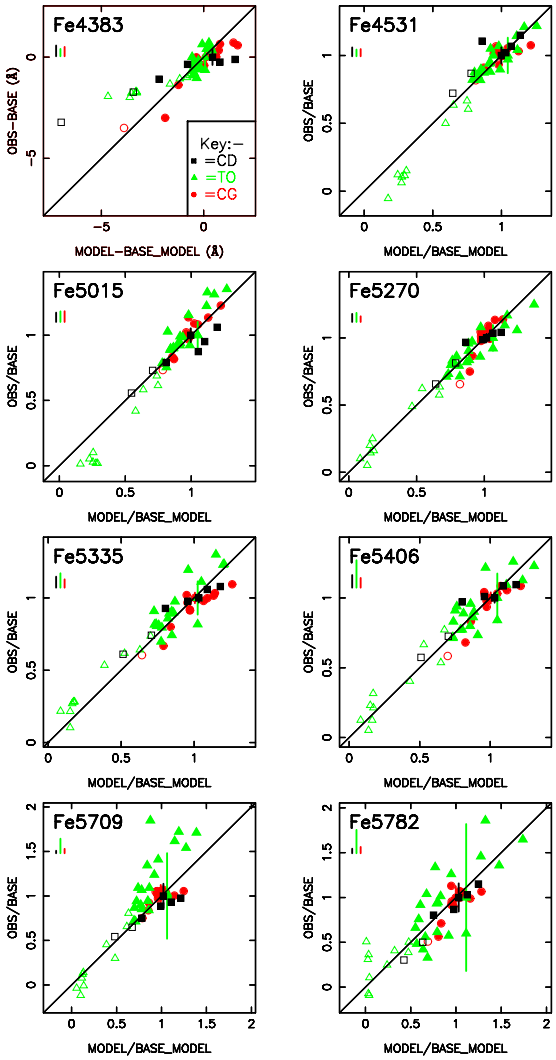

Figure 1(a). Testing the response functions of K05. Comparison of normalized empirical versus normalized theoretical line strengths for standard Lick indices sensitive to Fe lines in the stellar photospheres. (Note that Fe4531 and Fe5015 are more sensitive to overall metallicity [Z/H]; see K05.) The empirical observations are for stars in MILES, with known [Fe/H] and [α/Fe] (from [Mg/Fe] measurements in M11). Three star types are shown: cool dwarfs (CD, black squares), turn-off stars (TO, green triangles) and cool giants (CG, red circles). The observed stars shown are chosen to all have the same $T_{\rm eff}$ and $\log g$ as the base theoretical star within observational errors, for these three categories. The observed base stars used are HD 032147 (CD), HD 016673 (TO) and HD 154733 (CG), which match the atmospheric parameters tabulated for these three star types with solar abundance pattern in K05 (their tables 12, 13 and 14, respectively). Both empirical (vertical) and theoretical (horizontal) axes show either differences (for molecular bands and for lines indices that go negative or close to zero) or ratios (for indices that remain positive for all stars). Average observational errors (2σ) are attached to the base star points for each index. Systematic errors, estimated from observational uncertainties in base star atmospheric parameters, are indicated by the three vertical lines under the index name on each plot. These are colour coded for each star type modelled. For differences, these systematic error bars represent the maximum vertical offset expected because of combined line-strength uncertainties (added in quadrature), from uncertainties in $T_{\rm eff}$, $\log g$ and [Fe/H]; for ratios, these error bars indicate the slope uncertainty at one on the vertical axis because of these combined uncertainties. The straight line shows the one-to-one relation in each case. Open symbols show stars with [Fe/H] < -0.4, indicating stars with much lower metallicities than the base stars.

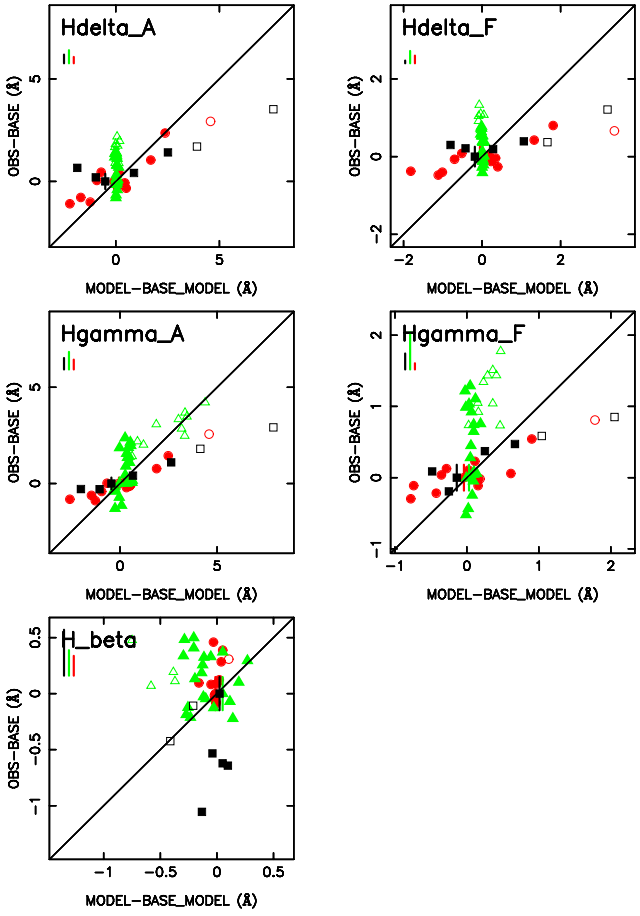

Figure 1(b). Testing the response functions of K05. Comparison of normalized empirical versus normalized theoretical line strengths for standard Lick indices sensitive to H Balmer lines in the stellar photospheres. Symbols as in Fig. 1(a), with cool dwarfs (CD, black squares), turn-off stars (TO, green triangles) and cool giants (CG, red circles).

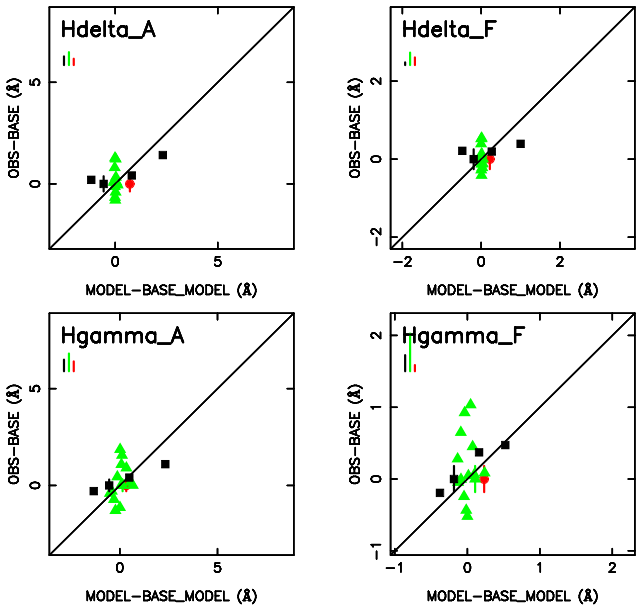

Figure 1(c). The same as the top four panels of Fig. 1(b), but for a restricted set of tested stars from MILES, which also have individual C, N and O abundance measurements applied.

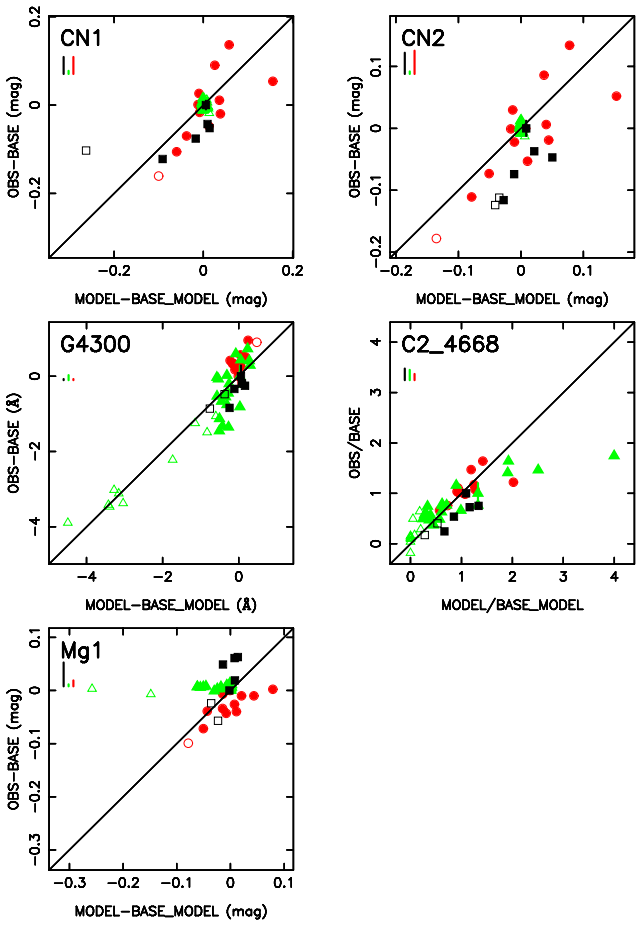

Figure 1(d). Testing the response functions of K05. Comparison of normalized empirical versus normalized theoretical line strengths for standard Lick indices sensitive to light metal (C, N and O) elements in the stellar photospheres. Symbols as in Fig. 1(a).

response functions are used in the literature, mainly by that group. In this section, we test the publicly available star response functions of K05 and H02, which are the ones most widely applied in the literature that we can test. We also test the star response functions used by L09, from information provided by G. Worthey (private communication, hereafter W12).

It is important to note that the published tables of response functions tested in this paper tabulate the responses of Lick spectral indices to changes in the abundance of individual elements, treating individual elements as trace abundances and assuming that the opacity distribution in the atmosphere is not significantly altered by changing the abundance of one element. However, the response-function tables (of TB95, K05 and H02) also tabulate changes in indices resulting from changes in overall metallicity [Z/H] and those values do take into account changes in the structure in the stellar atmospheres because of opacity changes. Because iron is a very important opacity source in stars, and is also most generally the element abundance measured in libraries of stars, we make use of these more self-consistent changes due to [Z/H] to go from theoretical base star indices to stars with different [Z/H] = [Fe/H] values. Then, we further adjust these index changes to account for non-solar abundance ratios relative to iron, treating the other elements (mostly α elements) as trace element changes. In this way, we aim to make best use of the physics that went into the models. For further discussion about the different order in which

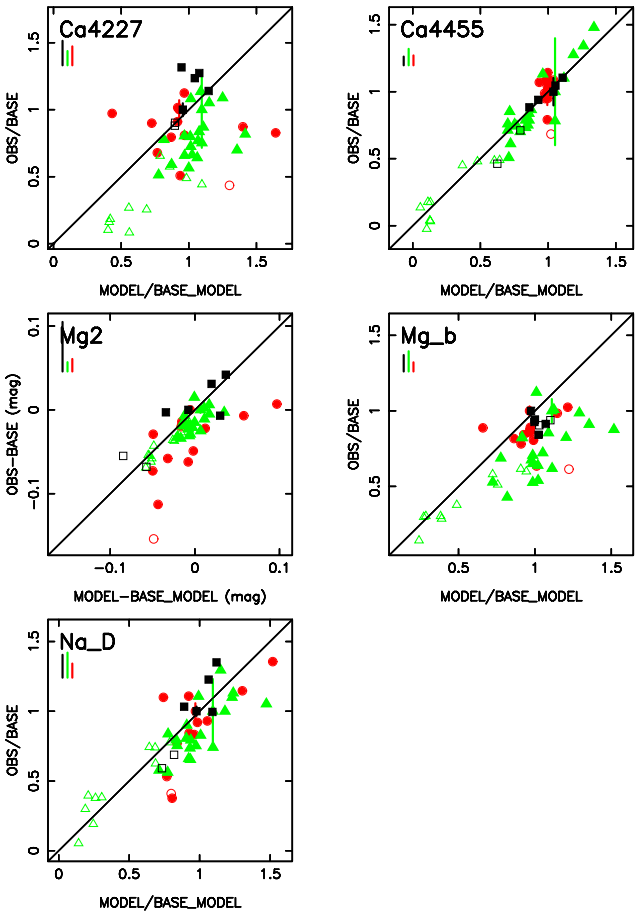

Figure 1(e). Testing the response functions of K05. Comparison of normalized empirical versus normalized theoretical line strengths for standard Lick indices sensitive to other elements in the stellar photospheres. For example, Ca4227 is most sensitive to Ca, Ca4455 is weakly sensitive to a variety of elements, Mg_2 and Mgb are most sensitive to Mg and NaD is most sensitive to Na. Symbols as in Fig. 1(a).

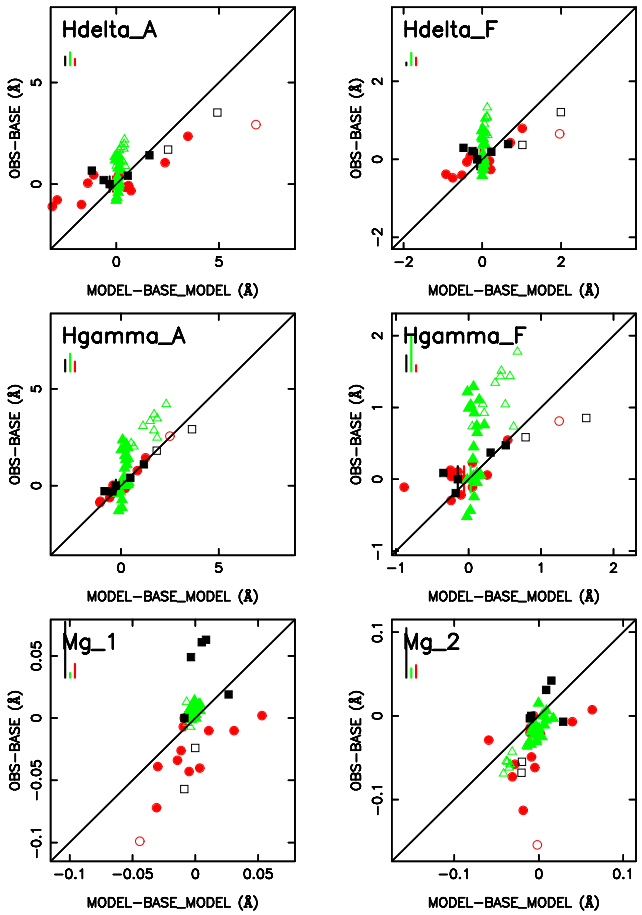

Figure 2. Testing the response functions of H02. Comparison of normalized empirical versus normalized theoretical line strengths for standard Lick indices sensitive to Hγ and Hδ Balmer lines, showing similar behaviour to that seen in Fig. 1(b); plus Mg_1 and Mg_2 indices. Symbols as in Fig. 1(a).

the response-function tables might be applied, see Proctor & Sansom (2002).

3.1 Response functions of K05

The response functions of K05 were generated from theoretical spectra blurred to the resolution of the Lick/IDS system, according to the resolution variations with wavelength measured by WO97 (see K05, section 2.4). Other corrections to the Lick/IDS standard system were not applied, which is the same approach as for the empirical observations that we are using here. Any remaining differences because of continuum normalization will be second-order effects, mainly affecting the broader band indices. The differential approach used in applying response functions will reduce the need for corrections because of differences in flux calibrations. However, we note that the broader spectral features are the ones most likely to show residual effects because of any remaining flux offsets. These are the CN, Mg and TiO bands.

3.1.1 Solar abundance pattern base models

Although K05 have presented response functions for base star models with different metallicities and some different abundance patterns, only those for base stars with solar abundances and solar abundance ratios can be tested here. This is because there are no suitable observed stars in MILES to match the specific base star models tabulated in K05 with non-solar abundances. That is, only tables 12– 14 (5-Gyr models) and tables 15 and 17 (1-Gyr models) in K05 have sufficient matching stars in MILES for us to be able to test them.

The theoretical model values are first derived from K05, using their tables 12, 13 and 14, which give element-dependent response functions for a CD, a TO and a cool giant (CG) star, respectively, from a 5-Gyr population, each of which starts with solar metallicity and abundance ratios. Base star parameters for these three models are shown in Table 3, together with matched observations used to make the normalized comparisons. We apply the response functions twice to the base models: once to generate a set of theoretical indices for the correct [Fe/H] for the star being modelled, by generating indices for a star with that overall [Z/H] (initially with solar abundance ratios), then again to modify those theoretical indices to the correct [α/Fe] of each of the observed stars being modelled. We enhance the α elements listed in Table 1, together with Na (see K05, section 2.1), whilst C, N, Cr and Fe remain unenhanced. We use this two-step process because there are insufficient observed stars of the specific $T_{\rm eff}$, log g, [Fe/H] combinations modelled, which could be used to isolate only [α/Fe] enhancement effects.

Table 3. Parameters for base stars that are used for normalizations in the response-function tests. The empirical parameters listed are for MILES base stars that match the base stars modelled by K05, within observational errors. These three stars are also modelled by H02. The maximum offsets assumed for this match are $\Delta T = \pm 100$ K, $\Delta \log g = \pm 0.2$, Δ[Fe/H] $= \pm 0.1$ and Δ[Mg/Fe] $= \pm 0.06$. The final column lists reference sources for the model or observation and also indicates the type of data available for the [Mg/Fe] determinations for each base star (see M11 for details).

Star type	Model or star name	$T_{\rm eff}$ (K)	log g	[Fe/H]	[Mg/Fe]	Source
CD	K05 table 12	4575	4.60	0.00	0.00	K05 & H02
CD	HD 032147	4658	4.47	+0.02	−0.06	M11 (HR)
TO	K05 table 13	6200	4.10	0.00	0.00	K05 & H02
TO	HD 016673	6253	4.28	+0.05	+0.05	M11 (HR)
CG	K05 table 14	4255	1.90	0.00	0.00	K05 & H02
CG	HD 154733	4200	2.09	0.00	−0.03	M11 (MR BothMg)

The observed stars chosen for the comparison are selected to be those that have the same atmospheric parameters of effective temperature and surface gravity as the tabulated theoretical model stars of K05, within the observational errors on these parameters. For the three base parameters, these errors are $\Delta T = \pm 100$ K, $\Delta \log g = \pm 0.2$ and Δ[Fe/H] $= \pm 0.1$ dex. For [Mg/Fe], we choose stars within Δ[Mg/Fe] $= \pm 0.06$ dex, because this is the main parameter that we are testing. Only specific base star models have response functions tabulated in K05, and therefore this determines our choice of stars that we can test. The observed $T_{\rm eff}$ and log g values are those given in the MILES spectroscopic data base (Cenarro et al. 2007), the observed [Fe/H] and [Mg/Fe] values are those given in M11 and the observed line strengths used are measured from MILES spectra convolved to the same spectral resolution as in K05 (as described in Section 2.3 and tabulated in Appendix A). Ratios (or differences) are then formed for both the observations (S) and corresponding theoretical model (M) indices. For a perfect match between observations and response-function predictions, the ratio M/S would equal 1 (or differences would equal zero):

$$\text{Ratio} = \text{M/S}. \tag{1}$$

Here,

$$M = \frac{M_*([\text{Fe/H}], [\alpha/\text{Fe}])}{M_*(0, 0)}$$

is the theoretical model ratio, and

$$S = \frac{S_*([\text{Fe/H}], [\alpha/\text{Fe}])}{S_*(0, 0)}$$

is the observed star ratio, where the denominators in M and S are the base star values.

The equations used to correct for different abundance patterns using the tabulated responses are from Thomas et al. (2003) (their equation 7) and K05 (their equation 3), for index and flux corrections, respectively. The equations used are described below.

Fractional changes in indices ($\Delta I/I_0$), as a result of the combined effects of tabulated response functions $R(i)$ for elements $i = 1$ to n, from Thomas et al. (2003, their equation 7) are

$$\frac{(I_{\rm new} - I_0)}{I_0} = \frac{\Delta I}{I_0} = \Pi_{i=1}^{n} \{\exp[R_{0.3}(i)]\}^{(\Delta[x_i]/0.3)} - 1, \tag{2}$$

where $R_{0.3}(i)$ are the tabulated fractional index changes for a factor of 2 increase in the abundance of element i, and $\Delta[x_i]$ is the change in the logarithmic abundance of element i (i.e. $\Delta[x_i] = +0.3$ for a factor of 2 increase in the abundance of element i).

Fractional changes in line fluxes ($\Delta F_{\rm l}/F_{\rm l0}$), as a result of the combined effects of index changes, from K05 (see their equation 3) are

$$\frac{(F_{\rm lnew} - F_{\rm l0})}{F_{\rm l0}} = \frac{\Delta F_{\rm l}}{F_{\rm l0}} = \Pi_{i=1}^{n} \left[\exp\left(\frac{\delta F_l}{F_{l0}}\right)\right]^{(\Delta[x_i]/0.3)} - 1, \tag{3}$$

where $\delta F_{\rm l}/F_{\rm l0}$ is the flux change for a factor of 2 increase in the abundances of element i.

The index and flux are linked via

$$I = W\left(1 - \frac{F_{\rm l}}{F_{\rm c}}\right), \tag{4}$$

where $F_{\rm c}$ is the continuum flux and W is the bandwidth for index I. This leads to

$$\frac{\delta F_{\rm l}}{F_{\rm l0}} = \frac{\delta I}{(I_0 - W)}, \tag{5}$$

as in equation (2) of K05, where $R = \delta I/I_0$ can be obtained from the tabulated response functions for specific elements and indices. Equation (5) can be used in general to convert from flux changes to index changes.

The corrections to indices are applied for those indices that behave as expected for weak lines (tending to zero strength for the weakest measurements), whereas corrections to fluxes are applied when the defined indices can take positive or negative values. This is to ensure that the property that is corrected for the element abundance pattern remains positive. After corrections are applied, fluxes are converted back to indices in order to make the comparisons with observations.

Figs 1(a)–1(e) show comparison plots for the response functions of K05. The stars plotted in these figures have a wide range in abundance pattern, covering $-2.86 <$ [Fe/H] $< +0.41$ and $-0.10 <$ [α/Fe] $< +0.53$. Stars with [Fe/H] < -0.4 are plotted as open symbols to highlight extrapolations to low metallicity, away from the base star model of [Fe/H] $= 0.0$.

To assess the significance of differences between observations and models, reduced chi-squared values were computed. Some systematic offsets from a one-to-one line in the comparison plots are expected because of slight mismatches between observed and theoretical base star parameters (see Table 3) This is unavoidable, because we have a finite number of observed stars and a finite number of base models for which theoretical response functions are available, and the two do not match perfectly. From the few suitable base stars available, it is found that these systematic offsets are generally small (typically less than twice the average errors on line strengths). They are larger for molecular band features, causing systematic shifts of up to ± 0.03 mag away from the one-to-one lines in the comparison plots. To estimate the size of systematic offsets expected because of uncertainties in atmospheric parameters of size $\Delta T = \pm 100$ K, $\Delta \log g = \pm 0.2$ and Δ[Fe/H] $= \pm 0.1$, we have used the MILES online interpolator (based on real stars),[2] to generate Lick indices for base stars, varying the parameters by these amounts. The average offsets in one direction are shown in Fig. 1, below the index name in each plot. These are shown for each of the three star types tested and represent a maximum typical systematic offset expected because of uncertainties in line strength, added in quadrature, as a result of the uncertainties in all three atmospheric parameters. For comparisons

[2] See http://miles.iac.es/pages/webtools/star-by-parameters.php.

Table 4. Reduced chi-squared (χ^2_ν) values for comparisons of normalized observations (from MILES) versus normalized models (using the response functions for [Z/H] and [α/Fe] changes in stars). These χ^2_ν values take into account errors added in quadrature from observational errors in Lick indices and systematic offsets partly as a result of slight base star mismatches. The results are shown for three star types (cool giant = CG, turn-off star = TO and cool dwarf = CD) and for star response functions from K05 and H02. The final column shows results comparing normalized observations versus normalized model, using star response functions for [α/Fe] changes only, as used by L09 (labelled ΔW12 here), for 71 stars in MILES.

Index number	Index name	χ^2_ν						
		K05			H02			ΔW12 only
		CG	TO	CD	CG	TO	CD	(any star type)
1	Hδ_A	4.61	1.75	10.57	17.81	1.76	6.71	5.09
2	Hδ_F	11.04	1.70	7.01	2.99	1.62	4.06	1.78
3	CN_1	7.96	1.02	7.52	8.78	0.61	1.15	14.58
4	CN_2	5.61	0.31	1.13	7.75	0.23	1.12	11.14
5	Ca4227	6.45	0.70	2.06	7.79	0.49	4.55	2.64
6	G4300	0.79	2.43	0.67	1.23	2.09	0.68	4.39
7	Hγ_A	8.18	3.96	5.88	0.48	2.23	1.40	9.92
8	Hγ_F	5.76	1.87	5.61	2.45	1.92	3.36	9.08
9	Fe4383	1.29	3.07	7.05	1.77	1.60	1.51	3.23
10	Ca4455	1.69	0.07	0.42	0.77	0.07	0.30	0.74
11	Fe4531	1.04	0.52	1.53	2.00	0.99	1.61	0.76
12	$C_2$4668	25.13	5.75	1.32	26.35	2.45	1.58	6.60
13	Hβ	1.12	2.25	1.69	1.66	1.65	1.28	1.32
14	Fe5015	1.19	1.49	1.52	1.14	1.49	6.68	3.02
15	Mg_1	2.06	4.80	3.00	1.69	1.12	9.27	16.46
16	Mg_2	1.94	1.70	12.07	2.23	1.28	12.69	32.91
17	Mgb	2.73	1.38	1.39	4.04	1.18	1.43	8.16
18	Fe5270	3.61	0.58	2.97	2.38	0.60	1.61	4.66
19	Fe5335	1.47	0.62	4.34	2.38	0.50	4.89	3.54
20	Fe5406	2.09	0.35	3.44	1.90	0.34	2.84	3.24
21	Fe5709	0.47	0.34	0.61	0.42	0.36	0.60	0.52
22	Fe5782	0.87	0.11	0.31	0.75	0.11	0.32	0.52
23	NaD	3.91	0.47	11.32	4.40	0.49	17.85	3.80

shown as differences, any inaccuracy in base star parameters will appear as a systematic offset above or below the one-to-one line in the comparison plots. For comparisons shown as ratios, any inaccuracy in the base star parameter will appear as a systematic fractional difference.

In order to generate error normalizations for evaluating chi-squared, average (2σ) errors from MILES, Lick indices were added in quadrature with mean offsets from the one-to-one line, for each index and each star type. This will account for offsets resulting from parameter inaccuracies in the base star, but not in the other stars, because the effect of such inaccuracies on Lick indices will be random rather than systematic. The reduced chi-squared (χ^2_ν) was found by dividing by the number of stars in each case, because no parameters were being fitted seeing as the comparison is with the one-to-one line prediction.

The results of the comparisons are described in Section 3.2 and the derived χ^2_ν values are given in Table 4.

3.2 K05 results

Fig. 1(a) shows the results for Lick indices mainly sensitive to Fe or overall metallicity. These indices show the expected behaviour for observed line-strength changes compared to theoretical ones. There are good one-to-one relations for the differential changes plotted between observations and those derived from theoretical response functions, given the observational errors. The agreement is confirmed by the reduced chi-squared values for these indices, which are typically $\chi^2_\nu < 3$ (see Table 4). Note that conservative 2σ error bars are plotted for the random Lick measurement errors. Therefore, they look larger than the typical data scatter for weak indices, such as Fe5782, where this Lick measurement error dominates the scatter. This agreement is not so surprising for features dependent mainly on Fe or overall metallicity, because these dominate spectral changes as a result of composition changes. Both systematic and random errors are generally larger for TO stars, because metal-sensitive line strengths are generally weak (and particularly sensitive to temperature uncertainties) in these warmer stars. Other systematic errors are relatively small, consistent with the good one-to-one relations seen in this figure.

Fig. 1(b) shows results for H Balmer Lick indices. For Hγ and Hδ, the K05 response functions do not mimic well what is happening in real stars as a function of changing abundance patterns ([Fe/H] and [Mg/Fe]). In the CD and CG stars, the theoretical response functions predict larger changes than are observed in the empirical star data. For the TO stars, the reverse is true, and the K05 response functions predict negligible variations in these indices as a function of changing abundance patterns (as highlighted, for example, in the vertical column of green triangles in the Hδ_A plot of Fig. 1b). Observed variations of Hγ and Hδ indices in these warmer stars are larger than the theoretical response functions predict. Some of the vertical scatter in these plots will result from inaccuracies in parameter measurements from star to star. Inaccuracies in base star parameters are not the cause of the systematic differences between observations and predictions, because that would cause systematic offsets rather than changes in slope around the mean, as observed in Fig. 1(b). This is confirmed by the relatively small systematic error bars for the cool stars, shown below the index labels on each plot. The differences between observations and predictions are highlighted by the large χ^2_ν values for CG and CD stars, for these higher-order Balmer indices (see Table 4).

The Hγ and Hδ indices are known to be affected by CN bands within the definition of these indices. Hγ_A might be sensitive to CH (i.e. G band) affecting its blue pseudo-continuum, whilst CN at 4150 Å might affect the red pseudo-continuum. Therefore, the difference, in principle, could be because of differences in C and N abundances, with carbon effects being particularly important in the response functions. Linear fits to the cool-star data ([Fe/H] ≥ -0.4) for Hγ and Hδ features in Fig. 1(b), give offsets that imply carbon abundance changes much larger than the maximum observed deviations in [C/Fe], which are $<\pm 0.4$ dex (e.g. Luck & Heiter 2006, 2007, hereafter LH06 and LH07). For example, for CG stars in Hγ_A, a shift of $+1.76$ Å would bring the lower point on to the 1:1 line, but this requires a change in [C/Fe] of 1.28 dex. Therefore, the slopes for cool stars in Fig. 1(b) cannot be reconciled with the 1:1 line by appealing to systematic changes in carbon abundance alone. Other aspects need to be considered. We have searched the literature for individual measurements of C, N or O abundances, relative to Fe, for the stars tested in Fig. 1(b), and we have found only a few. Fig. 1(c) shows the results of applying these individual abundance measurements. For the cool stars, there were only measurements of C and O for four CD stars (Luck & Heiter 2006) and C, N and O for one CG star (Luck & Heiter 2007). Abundances of C, N and O were available for 14 of the TO stars (Takeda & Honda 2005), which are also plotted. In Fig. 1(c), the response functions from K05 are applied as for Fig. 1(b), except that the columns for responses to individual C, N and O abundances are applied, where available, rather than their assumed links to [α/Fe] and [Fe/H] made previously, in Section 3.1.1. The systematic slope difference from

the 1:1 line, for five cool stars, is still evident in Fig. 1(c), and more measurements on individual C, N and O abundances are needed in future for further tests of the significance of the effects of these individual elements on the higher-order Balmer features.

We find, in Appendix B, that fine-tuning the abundance ratios, to take into account the mean trends of several elements, makes no significant difference to the mismatch for Hγ and Hδ indices, using the K05 response functions. This points to the overall metallicity response as the cause of the non-unity slopes for cool stars in these four indices (see Fig. 1b). For Hβ, the scatter is larger than expected from observational uncertainties in line strengths, because this index is thought not to be very sensitive to chemistry (e.g. L09; Cervantes & Vazdekis 2009, based on the synthetic stellar library of Coelho et al. 2005). However, note that a different conclusion for Hβ was reached by T07 and Cervantes & Vazdekis (2009), based on the synthetic stellar library of Munari et al. (2005). The offsets seen in Hβ can be explained by the systematic error bars plotted, which are particularly large for the CD stars in this index.

Fig. 1(d) shows Lick indices that are particularly sensitive to the light metals, C, N and O. These behave qualitatively as expected from the response functions, but with larger scatter than expected from the line-strength measurement errors in most cases. The χ^2_ν values reflect this (see Table 4). The lack of variation in the CN indices in TO stars, predicted from the theoretical response functions, agrees with the observations. For these CN indices in cool stars, errors resulting from atmospheric parameter uncertainties contribute to the scatter and offsets. Differences in CN band strengths between stars are also likely to contribute to this scatter. The Mg_1 feature, which is most sensitive to carbon, varies far more in the theoretical predictions than in the observations for the TO stars. Mg_1 in these warm TO stars is very weak compared to its values in the CD and CG stars and is observed to vary very little from star to star. Therefore, its theoretical response function is uncertain. Also, predicted ratios for $C_2$4668 extend to higher values for some TO stars than in the observations, which do not go above twice the base star line strengths in these stars. For $C_2$4668, in TO stars, the response-function predictions start to deviate significantly for applications to higher metallicities ([Fe/H] $> +0.2$), where the theoretical predictions have larger line strengths than the stellar observations, by up to a factor of 2, as seen in the extreme right TO star in Fig. 1(d) for the $C_2$4668 index. However, we note that in luminous elliptical galaxies, this index can take higher values (e.g. Zhu, Blanton & Moustakas 2010, see their fig. 14). Therefore, except for the weak Mg_1 feature in TO stars and for $C_2$4668 in TO stars, the response functions are not systematically biased in their predictions for these C-, N- and O-sensitive Lick indices (CN_1, CN_2, G4300, $C_2$4668 and Mg_1). Future high-resolution spectroscopic observations are needed to test the effects of C and N abundance variations on a star-by-star basis.

Fig. 1(e) shows Lick indices sensitive to other elements, including sodium and various α elements (Mg, Ca). Again, the response-function predictions are approximately followed by the observation, but with large scatter, and some offsets between star types. These systematic offsets shift vertically when different base stars are used, illustrating the sensitivity of these features to exact photospheric parameters, even within their observational uncertainties. The systematic error bars resulting from atmospheric parameter uncertainties are relatively large for most of these indices, as seen in this figure. The calcium-sensitive index Ca4227 shows large scatter about the one-to-one line, which might also reflect CN contamination effects (Schiavon 2007) and/or calcium variations that are not fully in step with magnesium variations in the observed stars, because we are using [Mg/Fe] as a proxy for all α elements (O, Ne, Mg, Si, S, Ar, Ca and Ti). In fact, there is evidence that calcium does not follow exactly in step with magnesium in a range of environments. For example, in our Galaxy, $0.0 <$ [Ca/Fe] $<$ [Mg/Fe] for metal-poor stars (Franchini et al. 2011) and calcium is even lower [Ca/Fe] ≤ 0.0 for open clusters (Pancino et al. 2010). Also, in luminous elliptical galaxies, calcium appears to follow iron rather than other α elements, such as magnesium (e.g. Vazdekis et al. 1997; Smith et al. 2009, and references therein). In future, it might be possible to compile calcium abundances on to a single scale, for a substantial number of MILES stars. Such a [Ca/Fe] catalogue would allow us to test whether differences in [Ca/Mg] are contributing to the scatter for some of the indices. This is particularly important for Ca4227, which currently shows poor agreement between response-function predictions and real stars. Ca4455 is weakly sensitive to a number of elements and the observations follow the response-function predictions well for this Lick index (see Table 4), with CG stars showing only small variations in both the observations and predictions.

The Mg_2 and Mgb indices, which are sensitive to magnesium, roughly follow the response-function predictions, but with quite large scatter and systematic offsets from the one-to-one relation. The variations in Na, sensitive to sodium, are qualitatively well predicted by the response functions, for all three star types, but with larger scatter than expected from Lick index uncertainties, for the cool stars.

The above results do not change significantly if different base stars are used, provided the base stars have the correct atmospheric parameters, within observational errors. This helps to confirm that the trends found are not just a result of small systematic differences in temperature scales between the theoretical and observed stars being compared. For the Mg indices (Mg_1, Mg_2, Mgb) and for Ca4227, in CG stars, differential index changes are slightly more affected by the choice of base star than in most cases. That is, the red circles in Figs 1(a)–1(e) shift significantly, compared to observational index errors, with a change in base star (systematically by $\sim\pm0.03$ mag for Mg_1 and Mg_2, and by $\sim\pm10$ per cent for Mgb and Ca4227). Therefore, for these indices, it is harder to accurately check the response-function predictions with the empirical observations.

A set of response functions for solar abundance models at the younger age of 1 Gyr are given in tables 15–17 of K05. Amongst the MILES stars, there are base stars that match the CD and CG model stars in these tables (but not for the TO model star). Therefore, comparisons were made of observed versus theoretical normalized indices for these younger CD and CG star models. Results have shown similar trends and scatters as previously found for the 5-Gyr models, but with a slight improvement in the $H\delta_A$ and $H\gamma_A$ indices, for which the normalized observations versus models were closer to one-to-one trends. Scatter for the Hγ and Hδ features increased in the comparisons for the younger age case.

In summary, most Lick indices follow the predictions of the K05 response functions as far as we can tell from the empirical data, except for $H\gamma_A$, $H\gamma_F$, $H\delta_A$ and $H\delta_F$ indices, which show systematic deviations from the predictions. These indices lie in the blue part of the spectrum where the flux from cool stars is rapidly changing with wavelength and where the influence of abundance effects is large (see Section 4). Similar results were found for two sets of MILES stars representing ages of 1 and 5 Gyr, respectively. The Mg_1 and $C_2$4668 indices also show systematic deviations from the response-function predictions in the case of warm TO stars, as described above.

3.3 H02 results

H02 have proposed an alternative set of models exploring response functions. They have made their response functions for models of three stars available at http://astro.wsu.edu/hclee/HTWB02. The H02 response functions differ in value from those of K05, and the line strengths listed at the base abundances are also slightly different. Here, the tables from H02 are used to test the same three stars as in tables 12–14 of K05 (in terms of their $T_{\rm eff}$ and $\log g$ parameter and base solar abundances). The same procedure as described in Section 3.1 was applied to test the H02 response functions. Overall, when compared to MILES observations, the results are very similar to what is found for the K05 response functions, with some improvements. Fig. 2 shows the Hγ and Hδ features using the H02 response functions, illustrating qualitatively the same problems as with the K05 response functions. However, we note that the H$\delta_{\rm F}$, H$\gamma_{\rm A}$ and H$\gamma_{\rm F}$ features for the H02 response functions give better agreement with the observations, as seen in Fig. 2 and in Table 4. Therefore, the use of H02 might be preferred over K05, particularly for the higher-order Balmer indices. Hβ has similar scatter for both the K05 and H02 cases. Table 4 also shows that the TO stars are generally better fitted by the H02 response functions.

For indices that are treated as positive, but which go slightly negative, the application of response functions becomes invalid. This is seen for $\rm Mg_1$ in TO stars, for K05 response functions (Fig. 1d), and for Hβ in CD and CG stars for H02 response functions. For the H02 response functions, the $\rm Mg_1$ index (expressed as a line strength) is positive for all three star types. Hence, TO stars show negligible variation in $\rm Mg_1$ in the model predictions, in agreement with the observations. Fig. 2 also shows plots for $\rm Mg_1$ and $\rm Mg_2$ from H02. The plot for $\rm Mg_2$ using the H02 response functions looks similar to that in Fig. 1(e) in spread and offsets (also true for Mgb), indicating similar results compared with those of the K05 response functions.

3.4 L09 results

L09 have noted that, in their models, the broader H$\gamma_{\rm A}$ and H$\delta_{\rm A}$ Balmer features are significantly affected by iron abundance. In their online comparisons with the K05 response functions for individual star models, their plot for H$\delta_{\rm A}$, for example, shows an increase of 2 Å (or 5.5 Å), for a +0.3 enhancement in [α/Fe] at constant [Fe/H] = 0.0 (or [Z/H] = 0.0);[3] red square (or blue square). It is difficult to compare this directly with the spread in observational data for this index, shown in Fig. 1(b), because those data include stars with a range of both [α/Fe] and [Fe/H] values. However, the spread in the observations is less than ∼5 Å over a broad range in composition, implying that the L09 models might also overestimate the variation expected in this index.

Although L09 have made use of extensions following from the work of H02, their online plots for individual star model response-function behaviour indicate different values than those in the H02 tables. Therefore, it would be very interesting to be able to test the star response functions of L09. However, L09 have not published tables of response functions for their 350 model stars (only for their SSPs). Therefore, the use of the L09 SSP response functions (their table 5) relies on the assumption that they have included different phases of stellar evolution in their correct proportions. This is likely to be better than the use of only three stars, as is often done in determining the response functions for SSPs. However, their published data do not allow us to test the understanding on a star-by-star basis, as we are attempting in this paper.

W12 has provided us with model response functions for stars and software used in L09 to generate index changes due to chemistry. These have allowed us to generate changes in indices for stars of user-defined atmospheric parameters. This information was used to derive three tables equivalent to tables 12–14 of K05, for changes due to individual elements in CD, TO and RG stars. For overall metallicity, the changes of K05 were assumed, because overall metallicity changes were not available in the W12 star response functions. Using these W12 response functions led to similar results as those found using the K05 response functions shown in Figs 1(a)–1(e), for individual stars. The discrepancies in the Hγ and Hδ indices remained. This similarity of results, using K05 overall metallicity changes with W12 changes to individual elements, supports the fact that overall metallicity is the dominant effect for most indices. That is, we are not finding different results using W12 changes to individual elements.

To probe the effects of [α/Fe] changes only, the W12 response functions were used as follows. Stars with [Mg/Fe] close to 0.0 (±0.01) in MILES were selected, providing 33 base stars. By matching stars in MILES with the same $T_{\rm eff}$, $\log g$ and [Fe/H] as these, within errors, but with differing [Mg/Fe], we obtained 80 matches. Of these, eight were associated with star clusters and were removed, because they generally had lower signal-to-noise. One other star with large [Mg/Fe] = +0.454 was also removed to avoid large changes in metallicity. The remaining stars all had |[Mg/Fe]| < 0.25. This latter restriction is applied here because these W12 response functions do not allow us to track the effects of overall metallicity changes, and therefore we can only use them to test trace element changes. Observed index differences for the remaining 71 stars were compared with index differences predicted from the W12 models. Fig. 3 shows the results for dwarfs stars (black squares, $\log g \geq 3.0$) and giant stars (red circles, $\log g < 3.0$). This shows data points scattering about the one-to-one line for each index, with little sign of any correlations, except in the case of magnesium and sodium ($\rm Mg_2$, Mgb, NaD), for which the correlation coefficients are 0.57, 0.48 and 0.43, respectively. These are significant at >99.9 per cent confidence levels, for 71 data points. For these few indices, there is evidence that observed index changes broadly follow index changes predicted by the W12 response functions. The Hγ and Hδ features show larger scatter than expected from the typical observational errors (particularly for the giant stars), but no systematic effects are evident that would imply an [α/Fe] dependence that is different between the observations and models. Mean offsets are all <0.2 dex. Some of the scatter in these differential [α/Fe] changes might be because the W12 response functions are evaluated from a specified [Fe/H] but keep overall metallicity constant. However, for the observed stars, their metallicity is characterized by [Fe/H] so we are not exactly comparing like with like, especially at increasingly non-solar [α/Fe]. Table 4 shows that the CN-, Hγ- and Mg-sensitive features agree least within the observational errors for these differential changes. Thus, the W12 response functions might be most useful for modelling the effects of element abundance changes, when they can be treated as trace element abundances changes. However, for the current comparisons, this runs into the finite errors on the [Mg/Fe] measurements, therefore weakening this test of the W12 response functions. More accurate measurements of abundances and responses of indices to overall metallicity would be needed to better test the response functions of W12, used in L09.

[3] See http://astro.wsu.edu/hclee/HdA.pdf.

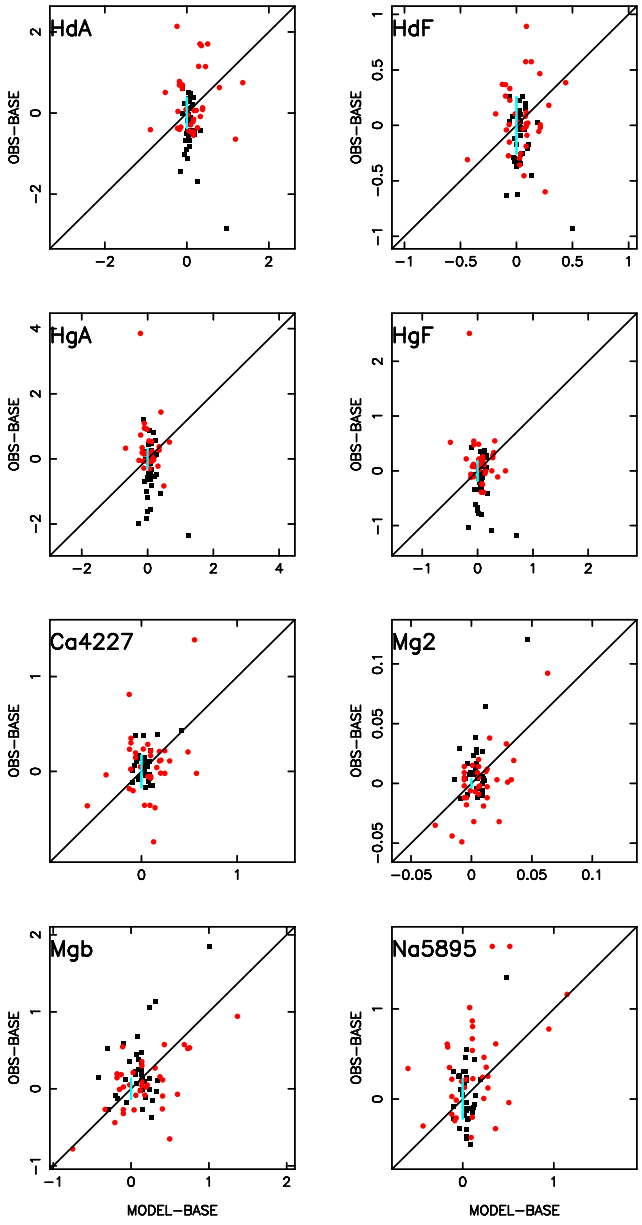

Figure 3. Testing the response functions of W12 for the effects of [α/Fe] changes only. Comparison of empirical versus theoretical line-strength differences for standard Lick indices in individual stars. The empirical observations are for stars in MILES, with known [Fe/H] and [α/Fe] (from [Mg/Fe] measurements in M11). This plot excludes open cluster stars and one star with |[Mg/Fe]| > 0.25. Two star types are shown, cool dwarfs (CD, black squares) and cool giants (CG, red circles), divided at $\log g = 3.0$. The observed stars shown are chosen to all have the same $T_{\rm eff}$, $\log g$ and [Fe/H] as the base stars within observational errors. The base stars used are from MILES and have [Mg/Fe] = 0.0, within a small tolerance of $\pm$0.01 dex. Average observational errors (2σ) are attached to one of the star points for each index. The straight line shows the one-to-one relation in each case. Both empirical (vertical) and theoretical (horizontal) axes show differences in Lick indices between observed stars and their matching base stars.

In summary, these results indicate that the systematic deviations seen in MILES observations relative to K05, for the Hγ and Hδ features, might result from insufficiently accurate accounting for the effects of overall metallicity changes in those response functions. The response functions of H02 agree slightly better with observations for those features. However, they are only available for three model stars. The star response functions of W12 provide the widest scope for testing trace element abundance changes but do not allow changes in overall metallicity to be easily tested. Therefore, there is, as yet, no particular set of response functions that provides the widest and best fit to star data. Caution should be exercised, particularly in interpreting the Hγ and Hδ indices in stellar populations, plus indices that reach values close to zero in some stars (Hβ, Mg$_1$) when using response functions.

4 COMPARISONS OF SPECTRA

Next, we test the attributes of spectra (rather than indices) to varying abundance patterns.

4.1 Comparison with published model spectra

Cassisi et al. (2004) were the first to compare their theoretical model spectra for enhanced and unenhanced stars. They found the largest differences in the blue part of the spectrum, particularly when comparing at constant overall metallicity.

In the current analysis, ratios were created for models of star spectra published by Coelho et al. (2005), for a typical dwarf star ($T_{\rm eff} = 5500$ K, $\log g = 4.0$, [Z/H] $= -0.2$) and a typical giant star ($T_{\rm eff} = 4500$ K, $\log g = 2.0$, [Z/H] $= -0.2$) for enhanced ([α/Fe] $= +0.4$) over unenhanced ([α/Fe] $= 0.0$) models, where α-elements are considered to be O, Ne, Mg, Si, S, Ca and Ti (see Coelho et al. 2005, section 3.1). The theoretical spectra are published at fixed [Fe/H] values and at these two [α/Fe] values. These spectra were interpolated to obtain spectra with overall metallicities at subsolar abundance [Z/H] $= -0.2$, using the transformations given by Coelho et al. (2007, see their table 1). This value of overall metallicity was chosen in order to maximize the possibility of finding similar enhanced and unenhanced stars in the observations. Hence, the model spectral ratios are compared in Fig. 4 with similar ratios, made from interpolating empirical dwarf star spectra in MILES, for particular values of [Fe/H] and [Mg/Fe]. The interpolator used is an extended version of the three-dimensional interpolator described by Vazdekis et al. (2003, 2010), which now allows the user to select stars by [Mg/Fe] (from M11), as a proxy for [α/Fe], within the limits imposed by the MILES coverage of this parameter. This also approximates the link from [Fe/H] to an estimate of overall metallicity [Z/H] by assuming the transformation given by Coelho et al. (2007, see their table 1). The empirical spectra used in Fig. 4 are approximate in enhanced [α/Fe] values, because of the limited range of such stars available in the local solar neighbourhood (as can be seen in fig. 10 of M11).

Qualitatively, we see good agreement between the theoretical and empirical spectral ratios plotted in Fig. 4. There are some differences in detail, particularly in the complex spectral region blueward of about 4500 Å. These are likely to be at least partially attributed to differences in C, N and O abundances between theoretical models and MILES stars. There are features modelled by Serven et al. (2005) that affect this region, including CNO3862 and CNO4175, as well as the CN bands and features due to other elements. New theoretical spectral models are currently being generated (Coelho, private communication) and a more quantitative comparison will await those models.

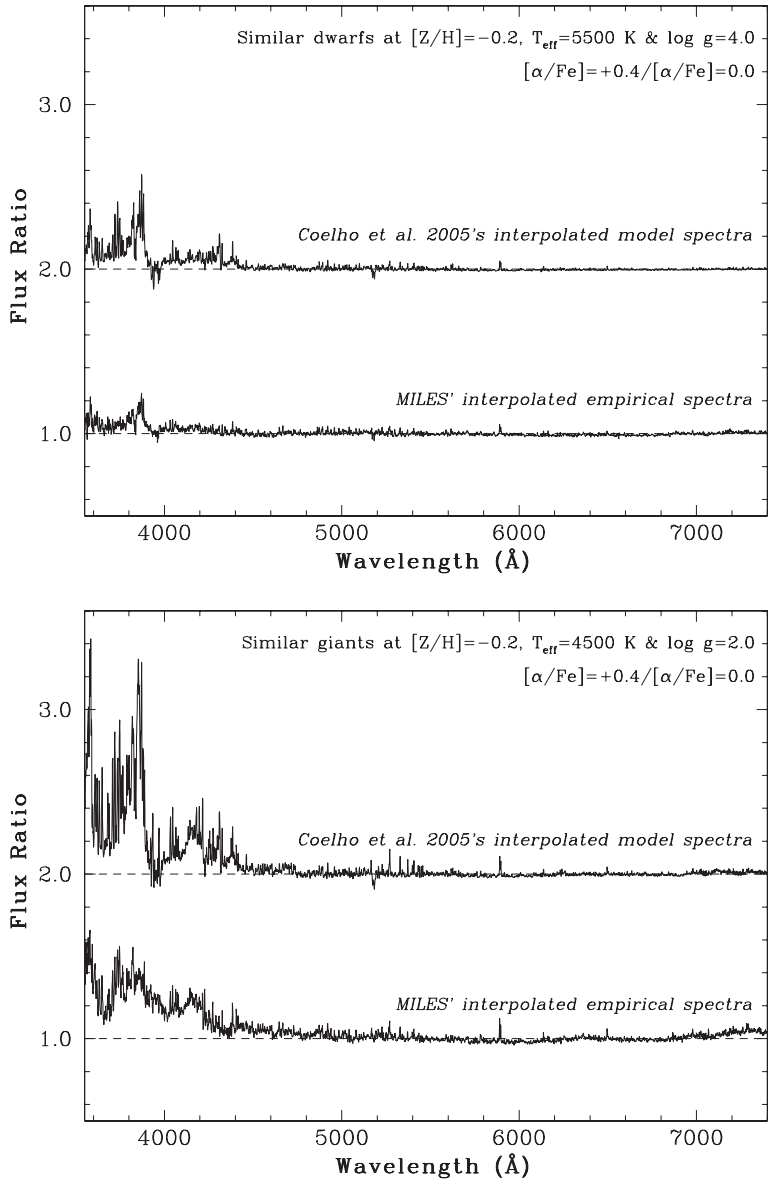

Figure 4. Comparison of the spectral ratios with enhanced ([α/Fe] = +0.4, [Fe/H] = −0.5) and unenhanced ([α/Fe] = 0.0, [Fe/H] = −0.2) abundance patterns, corresponding to fixed overall metallicity ([Z/H] = −0.2) in the models. Enhanced spectra are divided by unenhanced spectra in each case. The top plot shows dwarf stars ($T_{\rm eff}$ = 5500 K, log g = 4.0). The lower plot shows giant stars ($T_{\rm eff}$ = 4500 K, log g = 2.0). In each plot, the upper spectral ratio is theoretical, obtained by interpolating theoretical spectra from the library of Coelho et al. (2005) and the lower spectral ratio is observational, obtained by interpolating MILES. The theoretical spectral ratios are vertically offset by 1.0 to separate them from the observed spectral ratios shown.

4.2 Comparisons of empirical spectra for specific stars

To qualitatively investigate the influence of α-element abundance on empirical stellar spectra, stars were chosen in pairs with similar photospheric parameters in the MILES [Mg/Fe] catalogue (M11), for a few representative evolutionary stages in the context of SSP modelling. The evolutionary stages analysed are: a red normal giant with $T_{\rm eff} \approx 4000$ K and log $g \approx 1.5$ (around K5 III), a main-sequence TO star with $T_{\rm eff} \approx 6600$ K and log $g \approx 4.2$ (around F4 V) for an SSP of about 4 Gyr, and a cool main-sequence dwarf with $T_{\rm eff} \approx 5100$ K and log $g \approx 4.5$ (around K1 V).

The basic approach was to compute divisions of spectra by choosing pairs of similar stars in terms of $T_{\rm eff}$ and log g with different abundances, keeping [Z/H], [Fe/H] or [Mg/H] constant within some level. We have assumed the solar abundance pattern from Grevesse & Sauval (1998), as adopted by Coelho et al. (2005). We have calculated the overall [Z/H] from an abundance pattern, generating values for various combinations of [Fe/H] and [α/Fe], assuming all alpha elements are elevated to the same level. By fitting a bi-variable linear function to the results, we obtain the following transformation:

$$[{\rm Z/H}] = [{\rm Fe/H}] + 0.75(\pm0.02)[\alpha/{\rm Fe}] + 0.007(\pm0.006). \quad (6)$$

This is valid over the ranges $-1.5 \leq$ [Fe/H] $\leq +0.3$ and $-0.2 \leq [\alpha/{\rm Fe}] \leq +0.6$, and is accurate over this range to within $<\pm0.01$ dex (rms). This fitted equation gives very similar results to the correspondences tabulated by Coelho et al. (2007, see their table 1), which also assumed that all α elements varied in the same way. We have used the relation in equation (6) to search for pairs of stars in the MILES [Mg/Fe] catalogue (M11), assuming [α/Fe] = [Mg/Fe].

First, assuming [Z/H] constant (but [Fe/H] and [Mg/H] varying), spectra of MILES stars with larger and smaller values of [Mg/H] were divided. Then, considering [Fe/H] unchanged (but [Z/H] and [Mg/H] varying), spectral ratios of MILES stars were computed, with the larger divided by smaller [Mg/H]. To specifically evaluate the influence of [Fe/H] variation on the spectrum as well, spectral ratios were also obtained by changing [Fe/H] (and [Z/H]) with [Mg/H] constant. The spectrum of a MILES star with larger [Mg/Fe] (and smaller [Fe/H]) was divided by the spectrum of its analogue with smaller [Mg/Fe].

In this approach, any quantitative change in [Mg/H], [Fe/H] or [Z/H] for each comparison needs to be taken into account for a more precise analysis of the results. The differential relationship among the metal abundance parameters is $\mathrm{d[Z/H]} = \mathrm{d[Fe/H]} + 0.75\,\mathrm{d}[\alpha/\mathrm{Fe}]$, or

$$\mathrm{d[Z/H]} = 0.25\mathrm{d[Fe/H]} + 0.75\mathrm{d}[\alpha/\mathrm{H}], \quad (7)$$

in order to express all parameters on a scale relative to hydrogen.

Table 5 presents the set of star pairs adopted for each of the three evolutionary stages considered in the current spectral comparisons. We searched for pairs of similar stars in the MILES [Mg/Fe] catalogue with differences in $T_{\rm eff}$ and $\log g$ less than or equal to 50 K and 0.1, respectively. These fiducial values represent half of one standard deviation of the temperature and gravity errors for FGK stars in MILES (Cenarro et al. 2007). A very restrictive condition to fix [Z/H], [Fe/H] or [Mg/H] has also been imposed so that the maximum difference in each metal abundance parameter ($\Delta([\mathrm{X/H}])_{\rm max}$ is assumed to be $\leq$0.05 dex for each pair of stars. Gravity differences had to be relaxed in order to find some suitable pairs of stars, such that $\Delta\log g \leq 0.2$ for the red giants with fixed [Fe/H], $\leq$0.5 for CDs with [Fe/H] fixed and $\leq$0.3 for all TO stars. The abundance similarities also needed to be relaxed to $\Delta[\mathrm{X/H}] \leq 0.07$ for CDs.

4.2.1 *Normal red giant stage*

Considering [Z/H] fixed around the solar value, the more magnesium-enhanced red normal giant presents a flux excess in the blue part of spectrum (see Fig. 5a). This excess is a result of the increasing of [Mg/H] and/or decreasing [Fe/H]. However, when [Fe/H] is assumed constant, with [Z/H] changing below the

Table 5. Set of three pairs of similar MILES stars for (a) the red giant branch (RGB) stage, (b) the turn-off (TO) stage and (c) the cool dwarf (CD) stage. The first two rows in each of these evolutionary categories show the photospheric parameters of a pair of similar stars with fixed [Z/H] around the solar value but varying [Mg/Fe], [Mg/H] and [Fe/H] ($|\Delta([\mathrm{Mg/H}])| \geq 0.1$ dex). The intermediate two rows present the stellar parameters for a pair of similar stars with [Fe/H] fixed around the solar value but changing [Mg/Fe], [Mg/H] and [Z/H] ($|\Delta([\mathrm{Mg/H}])| \geq 0.25$ dex). In the last two rows, the parameters of another pair of similar stars are shown with [Mg/H] constant but varying [Mg/Fe], [Fe/H] and [Z/H] ($|\Delta([\mathrm{Fe/H}])| \geq 0.25$ dex). The parameters are from MILES, except that [Mg/H], [Mg/Fe], σ[Mg/Fe] and the notes are from M11; also, [Z/H] is from equation (6). The final column indicates whether [Mg/Fe] is from medium- or high-resolution spectral studies (see M11 for further details).

MILES	Type	Name	$T_{\rm eff}$ (K)	$\log g$	[Fe/H] (dex)	[Mg/Fe] (dex)	σMg/Fe (dex)	[Mg/H] (dex)	[Z/H] (dex)	Cat. notes
(a) Red giants										
[Z/H] constant										
0760F	Field	HD 192909	3880	1.34	−0.43	0.53	0.15	0.10	−0.03	MR Mg5528
0650F	Field	HD 164058	3902	1.32	−0.05	0.02	0.16	−0.03	−0.03	HR Ae01
[Fe/H] constant										
0059F	Field	HD 009138	4103	1.85	−0.37	0.19	0.10	−0.18	−0.22	MR BothMg
0557F	Field	HD 137704	4109	1.97	−0.37	−0.16	0.13	−0.53	−0.48	MR Mg5183
[Mg/H] constant										
0760F	Field	HD 192909	3880	1.34	−0.43	0.53	0.15	0.10	−0.03	MR Mg5528
0561F	Field	HD 139669	3895	1.41	−0.01	0.06	0.15	0.05	0.04	MR Mg5528
(b) Turn-off stars										
[Z/H] constant										
0444F	Field	HD 109443	6632	4.20	−0.65	0.43	0.10	−0.22	−0.32	MR BothMg
0525F	Field	HD 130817	6585	4.08	−0.46	0.14	0.10	−0.32	−0.35	MR BothMg
[Fe/H] constant										
0482F	Field	HD 119288	6594	4.03	−0.46	0.53	0.10	0.07	−0.06	MR BothMg
0412F	Field	HD 099747	6604	4.06	−0.51	0.16	0.10	−0.35	−0.38	MR BothMg
[Mg/H] constant										
0444F	Field	HD 109443	6632	4.20	−0.65	0.43	0.10	−0.22	−0.32	MR BothMg
0504F	Field	HD 125451	6669	4.44	0.05	−0.22	0.10	−0.17	−0.11	MR BothMg
(c) Cool dwarfs										
[Z/H] constant										
0145F	Field	HD 026965	5073	4.19	−0.31	0.34	0.12	0.03	−0.05	HR T98LH05
0684F	Field	HD 171999	5031	4.65	−0.10	−0.03	0.15	−0.13	−0.12	MR Mg5528
[Fe/H] constant										
0529F	Field	HD 132142	5108	4.50	−0.55	0.34	0.05	−0.21	−0.29	HR BM05
0138F	Field	HD 025673	5150	4.50	−0.60	0.07	0.05	−0.53	−0.54	HR BM05
[Mg/H] constant										
0750F	Field	HD 190404	5051	4.45	−0.17	0.39	0.05	0.22	0.13	HR BM05
0322F	Field	HD 075732	5079	4.48	0.16	0.09	0.05	0.25	0.23	HR BM05

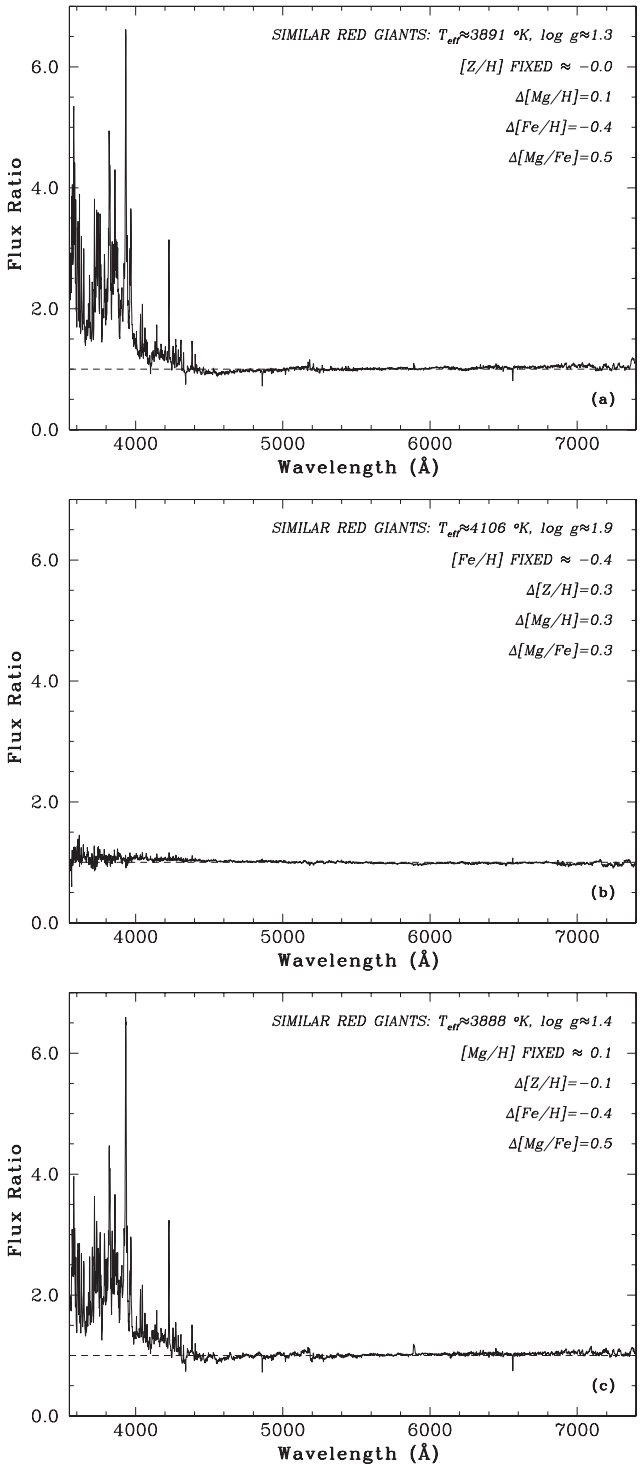

Figure 5. Ratios of pairs of MILES spectra of the following. (a) A pair of analogue stars for the RGB stage, fixing [Z/H] around the solar value but varying [Mg/H] and [Fe/H] (Δ([Mg/H]) = +0.13 and Δ([Fe/H]) = −0.38 dex). (b) A pair of analogue stars for the RGB stage, keeping [Fe/H] fixed slightly below the solar value but changing [Mg/H] and [Z/H] (Δ([Mg/H]) = +0.35 and Δ([Z/H]) = +0.26 dex). (c) A pair of analogue stars for the RGB stage, assuming [Mg/H] constant but varying [Fe/H] and [Z/H] (Δ([Fe/H]) = −0.42 and Δ([Z/H]) = −0.07 dex). The star names and their parameters are listed in Table 5.

solar value (Fig. 5b), the spectral ratio is relatively flat. By keeping [Mg/H] unchanged close to solar abundance and varying [Fe/H], the spectrum ratio shows that the excess in the blue flux is due to a smaller [Fe/H] (see Fig. 5c). The conclusion is that the blue flux excess for α-enhanced red giants in comparison with less α-enriched ones at a fixed overall metallicity [Z/H] occurs mainly because of a decrease in [Fe/H] instead of an increase in [α/Fe]. However, the level of this effect is uncertain in the data because the example shown uses an Algol-like system (HD 192909). There is some limited capacity to check this result with other pairs of similarly cool red giant stars in MILES. The spectral ratios found vary, but qualitatively show the same results in most cases. Hotter red giant stars show less variation (also see Section 5). This analysis is also limited by the observational errors on all photospheric parameters involved, as qualitatively stressed for temperature and gravity, later in this section. Therefore, we have attempted to concentrate on the most reliable cases.

4.2.2 *Main-sequence turn-off dwarf for an evolved SSP*

By following a similar procedure for three pairs of TO stars, we can show that they vary much less with abundance changes, but still vary most in the blue. The results are shown in Fig. 6, with a smaller vertical scale than that used for the red giants in Fig. 5. This smaller variation as a result of chemistry is not so surprising because these are hotter stars (see Section 5). A few other similar pairs of stars show qualitatively similar behaviour.

4.2.3 *Cool main-sequence dwarf*

Spectral ratios for three pairs of CD stars are plotted in Fig. 7 with the same vertical scale as for the TO stars in Fig. 6. Variations are smaller than for the cool RG stars, but greater than for the warm TO stars. When [Fe/H] is kept fixed (central plot in Fig. 7), there are the least variations in the blue. When [Mg/H] is kept fixed (lowest plot in Fig. 7), there are small variations, particularly in the blue, mainly because of changes in [Fe/H]. A few similar examples can be found in the MILES data, qualitatively supporting the relative behaviour shown in Fig. 7.

In future, these spectral ratios will be compared with their exact counterparts in the new theoretical models currently being generated.

4.2.4 *Effect of parameter errors on spectrum ratios*

We have investigated the impact of errors in $T_{\rm eff}$ and $\log g$ on the flux ratios of similar stars. In MILES, the typical uncertainty for FGK stars is 100 K in temperature and 0.2 in $\log g$. To analyse the influence of significant temperature and surface gravity deviations, we computed spectrum ratios for selected pairs of analogue stars with very similar parameters, except for temperature (which deviated by ≥275 K) and log gravity (which deviated by ≥0.6).

For cool giants, a temperature increase of more than three times the temperature uncertainty produces more blue flux (from 20 per cent upwards) and residuals in lines across the spectrum, all appearing as excesses or deficiencies in the spectrum ratios. The difference dominates in the blue, but the whole spectrum is affected to some extent. Flux ratios analysed for pairs of RGB stars do not exhibit this pattern that results from such $T_{\rm eff}$ deviations. Also, the pattern of effects produced by $\log g$ uncertainties are not seen in the RGB flux ratios (see Fig. 5). For the TO stars, the effects of these uncertainties in temperature and gravity are not significant, except

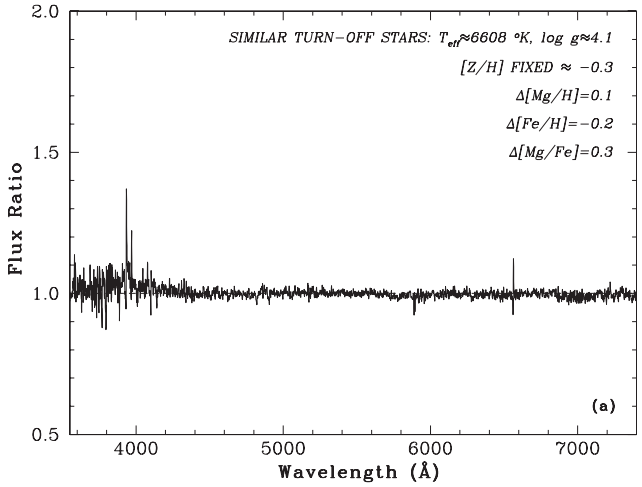

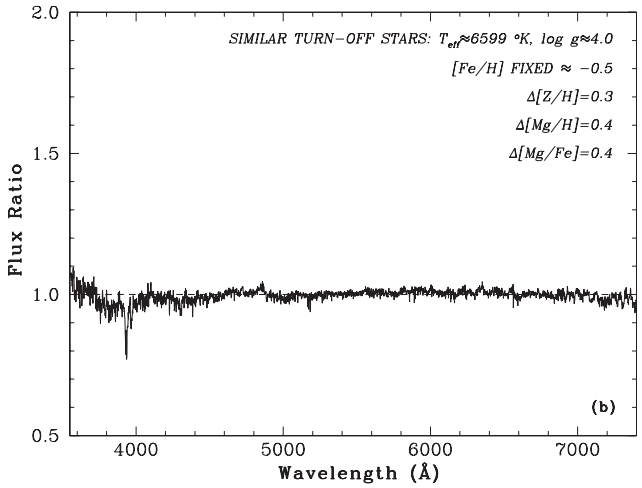

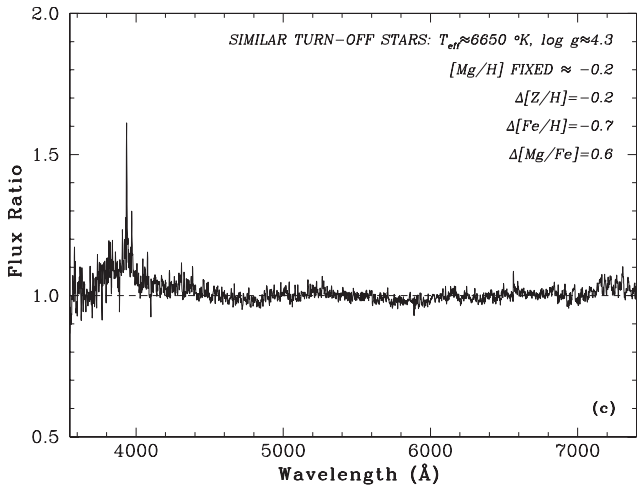

Figure 6. Ratios of pairs of MILES spectra of the following. (a) A pair of analogue stars for the TO stage, fixing [Z/H] below the solar value but varying [Mg/H] and [Fe/H] (Δ([Mg/H]) = +0.10 and Δ([Fe/H]) = −0.19 dex). (b) A pair of analogue stars for the TO stage, keeping [Fe/H] fixed below the solar value but changing [Mg/H] and [Z/H] (Δ([Mg/H]) = +0.42 and Δ([Z/H]) = +0.44 dex). (c) A pair of analogue stars for the TO stage, assuming [Mg/H] constant but varying [Fe/H] and [Z/H] (Δ([Fe/H]) = −0.70 and Δ([Z/H]) = −0.21 dex). The star names and their parameters are listed in Table 5.

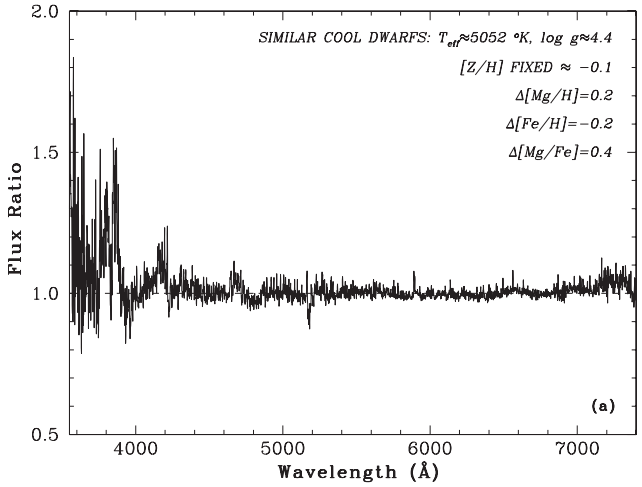

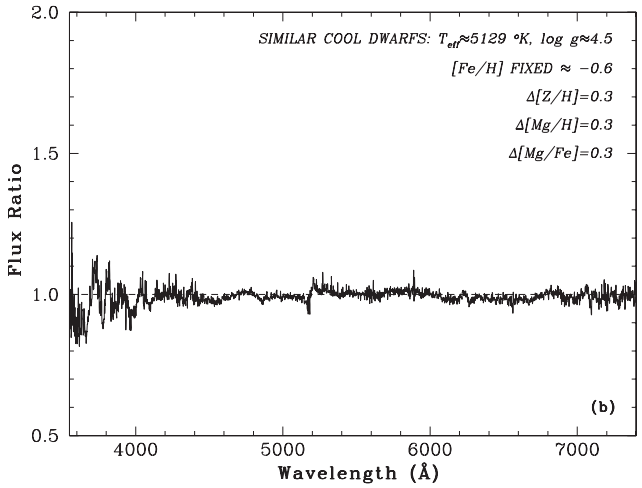

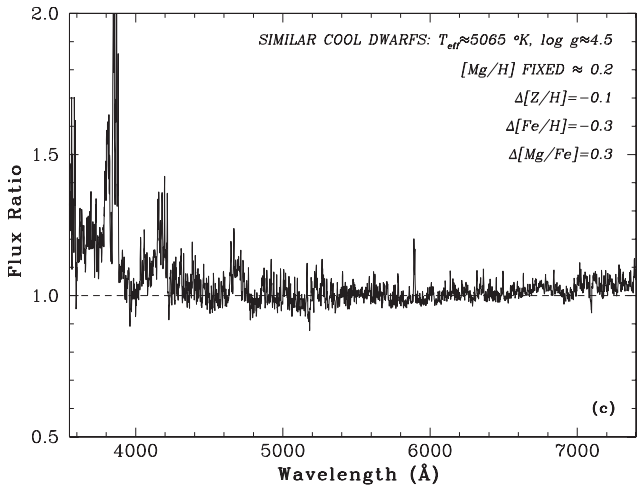

Figure 7. Ratios of pairs of MILES spectra of the following. (a) A pair of analogue stars for the CD stage, fixing [Z/H] around the solar value but varying [Mg/H] and [Fe/H] (Δ([Mg/H]) = +0.16 and Δ([Fe/H]) = −0.21 dex). (b) A pair of analogue stars for the CD stage, keeping [Fe/H] fixed below the solar value but changing [Mg/Fe] and [Z/H] (Δ([Mg/H]) = +0.32 and Δ([Z/H]) = +0.25 dex). (c) A pair of analogue stars for the CD stage, assuming [Mg/H] constant but varying [Fe/H] and [Z/H] (Δ([Fe/H]) = −0.33 and Δ([Z/H]) = −0.10 dex). The star names and their parameters are listed in Table 5.

that the Ca II H & K lines just below 4000 Å are affected by changes in both log g and $T_{\rm eff}$ at some level. (Perhaps they affect the spectrum ratios shown in Fig. 6, especially in Fig. 6(c), which shows the constant [Mg/H] case.) The impact of temperature uncertainties on the CD spectrum ratios exhibits qualitatively similar behaviour as in the RGB case, but with a smaller magnitude because the CD stars are hotter. There is no significant effect of gravity uncertainty on flux ratios for the CD case, except for the constant [Fe/H] case, where the spectrum ratio is close to one throughout (Fig. 7 b). Therefore, we are confident that the differences that we are seeing in Figs 5, 6 and 7 are not dominated by $T_{\rm eff}$ and log g parameter uncertainties in these MILES similar star pairs.

4.2.5 Influence of C, N and O abundances on [Z/H] estimation

The CNO group is an important contributor to the total metal content and integrated opacity in a stellar photosphere. To investigate the impact of individual abundances of C, N and O on the global metallicity estimate, we recomputed [Z/H] on a star-by-star basis (for the stars listed in Table 5), adopting their published abundances where available. When there is no elemental abundance available or if the star's collected [Fe/H] does not match its MILES value (within 2σ[Fe/H] = 0.2 dex), we estimated [X/Fe] from observed mean galactic trends for local disc stars. In Table 6, we compile the individual re-estimated [Z/H] as well as the CNO abundances. This approach should be more precise than the previously applied approximation (equation 6), in which the α-element abundances (including oxygen) are all represented by magnesium, with carbon and nitrogen assumed to be scaled-solar. The galactic trends of [C/Fe] and [N/Fe] as a function of [Fe/H] for dwarf stars are those from Takeda & Honda (2005), that is, [C/Fe] $= -0.21(\pm0.03)$[Fe/H] $+ 0.014(\pm0.006)$ and [N/Fe] around the solar value (obtained from a sample of 160 nearby FGK dwarfs/subgiants with $-0.7 \leq$ [Fe/H] $\leq +0.4$). The trends of [O/Fe] for dwarfs and [C,N,O/Fe] for giants are listed in Appendix B (Table B1) and illustrated in Fig. B1; these are from Soubiran & Girardi (2005), hereafter SG05, and LH07, respectively.

According to our simpler procedure to estimate [Z/H], the variation in [Z/H] is linearly correlated to the variations in [Fe/H] and [α/H] (equation 7). To evaluate how the individual CNO abundances modify this approximation, we checked whether Δ[Z/H], Δ[Fe/H] and Δ[α/H] (Mg or O as a proxy) follow this differential relationship, considering typical abundance errors (about 0.1 dex on average). In summary, our main results are as follows for the pairs of similar stars given in Table 5; the differences in estimated [Z/H] values are plotted in Fig. 8.

[Z/H] constant. Δ[Fe/H], accounting for the small variations in [Z/H] (of 0.08 and 0.13 dex in the RG and TO stars, respectively), is better correlated with Δ[O/H] instead of Δ[Mg/H]. For the CD case, the variation in [Z/H] is very close to zero.

[Fe/H] constant. The expected correlation d[Z/H] $= 0.75$d[α/H] from equation (7) works (within the abundance uncertainties), except that the two RG stars show the largest deviations, as plotted in Fig. 8.

[α/H] constant. The variation in [Fe/H] correlates well with Δ[Z/H] following our simple approximation in equation (7). For the TO case, the relation would be better reproduced if [α/H] differences, in elements other than Mg, were allowed for. In the CD case, the differential relationship (equation 7) would be acceptable if the outlying data from Zhao et al. (2002) were excluded (see their [O/H] value in Table 6).

In general, we find that the few available C, N and O individual abundances have some influence on the estimation of overall metallicity [Z/H], but this is not a significant effect, taking into account the abundance uncertainties; there are only two stars that deviate from equation (7) by 2–3σ [Fe/H], both from the [Fe/H] constant case of RG stars, where [O/H] does not follow [Mg/H] (see Fig. 8). Only one stellar spectral comparison is probably invalid: the [α/H] constant case of TO stars. Thus, our standard approach expressed by equations (6) and (7) can be considered as a reliable approximation of [Z/H] for the present analysis. However, by adopting well-determined CNO abundances in a homogeneous system, we will provide more precise global metallicity estimates in future. We will be able to redo the spectral-ratio analysis when we have completed an abundance compilation for as many MILES stars as possible. An important aspect of this task will be to transform all [X/Fe] on to a uniform system, checking the scales of $T_{\rm eff}$, log g and [Fe/H] of each referenced work against the MILES system of parameters. This is a longer-term project that is currently in progress.

5 DISCUSSION

The uncertainties in response functions can lead to different predictions for stellar population ages as well as for abundances. For example, for a CG star, an increase in [α/Fe] of +0.3 at fixed [Fe/H] = 0.0 leads to predicted changes in H$\delta_{\rm F}$ of +0.56 Å (from K05 response functions) and +0.36 Å (from H02 response functions), a difference in predictions of ΔH$\delta_{\rm F} = +0.20$ Å. Alternatively, using response functions for overall [Z/H], then lowering the Fe-peak elements and C back down to solar leads to predicted changes in H$\delta_{\rm F}$ of −0.08 Å (from K05 response functions) and +0.32 Å (from H02 response functions). The difference between these predictions is thus ΔH$\delta_{\rm F} = +0.40$ Å. This is significant when compared with changes in H$\delta_{\rm F}$ expected with age in SSPs (at 5 Gyr, [Fe/H] = 0.0), as shown by Schiavon (2007, see their fig. 7): age increases by ∼3 Gyr for a drop of 0.4 Å in H$\delta_{\rm F}$. Thus, the larger predicted increase in H$\delta_{\rm F}$ from K05 response functions would result in a slightly older age estimate, because more of the H$\delta_{\rm F}$ increase is explained as being the result of abundance ratio effects in this case.

This effect is diluted when a range of stellar types is considered in the calculations. Following the luminosity weighting combination used by Trager et al. (2000) (53, 44 and 3 per cent of the light from CG, TO and CD stars, respectively, approximating a 5-Gyr population), we raise only the α-element group by +0.3 in the log and find a difference of ΔH$\delta_{\rm F} = +0.07$ Å, between the K05 and H02 response-function predictions. This corresponds to a change in age of less than 1 Gyr. Larger differences between the K05 and H02 predictions are found when the [Z/H] column of the response functions is used (as discussed in Section 3), which can lead to significant age uncertainties for an SSP.

Deviations for the higher-order Balmer features in cool stars, seen in Fig. 1(b), correlate more strongly with the metallicity of the stars (characterized by [Fe/H]) than they do with [Mg/Fe]. We used the column for overall [Z/H] changes in the response functions tested in Figs 1 and 2, in order to reach the correct [Fe/H] values (for solar abundance ratios), before modifying the index changes due to non-solar abundance ratios using the α-element columns of the response-function tables. Therefore, it is likely that the most uncertain response-function predictions for these features in K05 are the ones tabulated for [Z/H] changes. More accurate theoretical predictions for these changes are needed in the blue part of the spectrum in order to make accurate predictions of how Hγ and Hδ

Table 6. C, N and O data for pairs of similar stars (corresponding to those in Table 5). The references cited are: LH07, Luck & Heiter (2007); GL93, Garcia Lopez et al. (1993); LH06, Luck & Heiter (2006); PM11, Petigura & Marcy (2011); Re07, Ramírez, Allende Prieto & Lambert (2007); Ee04, Ecuvillon et al. (2004); Ce06, Casagrande, Portinari & Flynn (2006); DM10, Delgado Mena et al. (2010); Ze02, Zhao et al. (2002); Ee06, Ecuvillon et al. (2006). For galactic trend estimates only: $[X/H] = [Fe/H]_{MILES} + [X/Fe]_{Trend}$; otherwise $[X/H] = [Fe/H]_{Ref} + [X/Fe]_{Ref}$. Mean galactic trends of [X/Fe] as a function of [Fe/H] for local disc stars: giants C & N (Takeda & Honda 2005); O (SG05); dwarfs C, N and O (LH07).

Name	[Fe/H] (MILES) (dex)	[Mg/Fe] (MILES) (dex)	[Mg/H] (MILES) (dex)	[Fe/H] (dex)	[C/Fe] (dex)	[C/H] (dex)	Ref. or trend	[N/Fe] (dex)	[N/H] (dex)	Ref. or trend	[O/Fe] (dex)	[O/H] (dex)	Ref. or trend	Notes	[Z/H] new (dex)
Red giants															
[Z/H] constant															
HD 192909	−0.43	0.53	0.10		0.03	−0.40	Trend	0.15	−0.28	Trend	0.38	−0.05	Trend		−0.10
HD 164058	−0.05	0.02	−0.03		−0.14	−0.19	Trend	0.20	0.15	Trend	0.07	0.02	Trend		−0.02
[Fe/H] constant															
HD 009138	−0.37	0.19	−0.18	−0.34	0.19	−0.15	LH07	0.15	−0.19	LH07	0.52	0.18	LH07	CNO	0.01
HD 137704	−0.37	−0.16	−0.53		0.01	−0.36	Trend	0.16	−0.21	Trend	0.32	−0.05	Trend		−0.19
[Mg/H] constant															
HD 192909	−0.43	0.53	0.10		0.03	−0.40	Trend	0.15	−0.28	Trend	0.38	−0.05	Trend		−0.10
HD 139669	−0.01	0.06	0.05		−0.15	−0.16	Trend	0.20	0.19	Trend	0.05	0.04	Trend		0.01
TO stars															
[Z/H] constant															
HD 109443	−0.65	0.43	−0.22		0.15	−0.50	Trend	0.00	−0.65	Trend	0.25	−0.40	Trend		−0.40
HD 130817	−0.46	0.14	−0.32		0.11	−0.35	Trend	0.00	−0.46	Trend	0.26	−0.20	GL93	O	−0.27
[Fe/H] constant															
HD 119288	−0.46	0.53	0.07		0.11	−0.35	Trend	0.00	−0.46	Trend	0.25	−0.21	Trend	[a]	−0.19
HD 099747	−0.51	0.16	−0.35		0.12	−0.39	Trend	0.00	−0.51	Trend	0.25	−0.26	Trend		−0.32
[Mg/H] constant															
HD 109443	−0.65	0.43	−0.22		0.15	−0.50	Trend	0.00	−0.65	Trend	0.25	−0.40	Trend		−0.40
HD 125451	0.05	−0.22	−0.17		0.00	0.05	Trend	0.00	0.05	Trend	−0.19	−0.14	GL93	O	−0.07
Cool dwarfs															
[Z/H] constant															
HD 026965	−0.31	0.34	0.03	−0.24	0.14	−0.10	LH06	0.00	−0.31	Trend	0.12	−0.12	LH06	CO	−0.15
				−0.28	0.08	−0.23	Trend	0.00	−0.31	Trend	0.38	0.10	PM11	O	−0.02
				−0.31	0.08	−0.23	Trend	0.00	−0.31	Trend	0.41	0.10	Re07	O	0.00
				−0.31	0.42	0.11	Ee04	0.00	−0.31	Trend	0.23	−0.08	Trend	C	−0.02
HD 171999	−0.10	−0.03	−0.13		0.03	−0.07	Trend	0.00	−0.10	Trend	0.16	0.06	Trend	[b]	−0.01
[Fe/H] constant															
HD 132142	−0.55	0.34	−0.21	−0.54	0.13	−0.42	Trend	0.00	−0.55	Trend	0.24	−0.30	Ce06	α	−0.33
				−0.45	0.13	−0.42	Trend	0.00	−0.55	Trend	0.51	0.06	PM11	O	−0.17
					0.13	−0.42	Trend	0.00	−0.55	Trend	0.25	−0.30	Trend		−0.33
HD 025673	−0.60	0.07	−0.53	−0.53	0.14	−0.46	Trend	0.00	−0.60	Trend	0.15	−0.38	Ce06	α	−0.48
				−0.50	0.32	−0.18	DM10	0.00	−0.60	Trend	0.15	−0.35	DM10	CO	−0.42
					0.14	−0.46	Trend	0.00	−0.60	Trend	0.25	−0.35	Trend		−0.42
[Mg/H] constant															
HD 190404	−0.17	0.39	0.22		0.05	−0.12	Trend	0.00	−0.17	Trend	0.19	0.02	Trend		0.02
HD 075732	0.16	0.09	0.25	0.32	−0.02	0.14	Trend	0.00	0.16	Trend	0.04	0.36	Ze02	O	0.19
				0.31	−0.02	0.14	Trend	0.00	0.16	Trend	−0.18	0.13	PM11	O	0.09
				0.33	−0.02	0.14	Trend	0.32	0.65	Ee04	−0.05	0.11	Trend	N	0.18
				0.33	−0.02	0.14	Trend	0.00	0.16	Trend	−0.20	0.13	Ee06	O	0.09
					−0.02	0.14	Trend	0.00	0.16	Trend	−0.05	0.11	Trend		0.15

[a] One work, [Fe/H] deviates from MILES (HD 119288; Clementini et al. 1999).
[b] Two works, [Fe/H] deviates from MILES (HD 171999; PM11; Trevisan et al. 2011).

absorption features should vary with overall metallicity and with [Fe/H].

Another area of uncertainty is how individual elements might vary on a star-to-star basis and the effect that this might have on the current comparisons. To address this question more accurately, it will be important in future work to obtain high spectral resolution observations for all these tested stars.

At present, the best agreement is with the H02 response functions for the higher-order Balmer features. Therefore, the use of these is recommended, particularly for age determinations using these features. In future, more comprehensive response functions are needed for a wider range of star types, utilizing more accurate theoretical predictions in the blue part of the spectrum.

Hβ shows larger than expected scatter, particularly for the TO stars (green triangles in Fig. 1b). The sensitivity of this index to abundance pattern variations needs further study, because there are conflicting results between current theoretical models (e.g. Coelho et al. 2005; Munari et al. 2005).

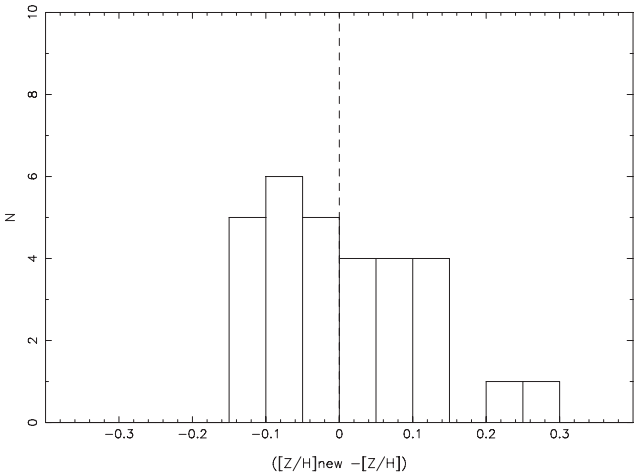

Figure 8. Histogram of differences between [Z/H] new (derived using individual C, N, O, Mg and Fe abundances from Table 6) and [Z/H] estimated using equation (6).

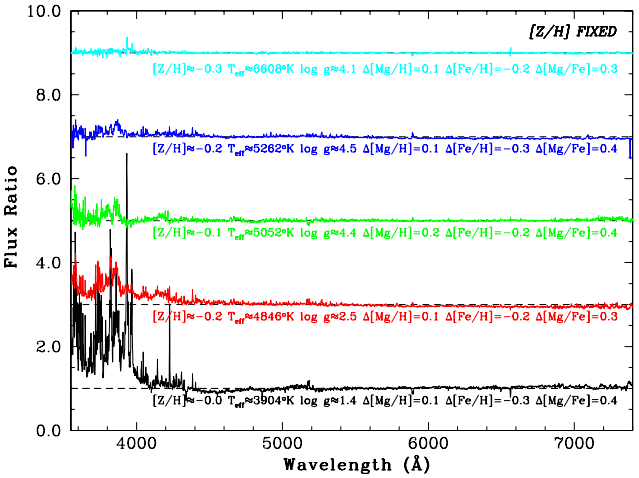

Figure 9. Ratios of pairs of MILES spectra showing the increasing importance of abundance pattern variations for cooler temperature stars. The plots are at fixed [Z/H] (typically around −0.2, estimated using equation 6), but varying [Mg/H] and [Fe/H], and are successively offset by 2.0 to avoid overlap. The star parameters are listed under each plot.

Another important feature, whose behaviour with abundance pattern variations is not well reproduced by the response functions of K05 (or H02), is Ca4227, which is sensitive to calcium. There is a large scatter between theoretical predictions and empirical measurements for this feature (see Fig. 1e). This feature has been used in the past to conclude that giant ellipticals are underabundant in calcium (i.e. [Ca/Mg] < 0.0) and hence that calcium follows iron more closely in those galaxies (Vazdekis et al. 1997; Cenarro et al. 2004). However, the lack of good predictions of Ca4227 line strengths in stars in the local solar neighbourhood, as seen in Fig. 1(e), calls into question the accuracy of the response functions for this feature. This feature is thought to be affected by CN bands (Prochaska, Rose & Schiavon 2005). Therefore, to interpret it accurately, it might be that the CN band strength also needs to be accurately predicted, and any assumption about the behaviour of C or N might lead to inaccurate conclusions about the interpretation of the Ca4227 line strength. There is a weak trend of increasing offsets below the 1:1 line, with increasing [Mg/Fe] for Ca4227, which also hints at additional abundance dependences that are not yet fully accounted for in the response functions for this feature. The magnesium-sensitive features (Mg_2 and Mgb) show more of a correlation with theoretical expectations (in Figs 1e and 2 for K05 and H02 response functions, respectively). However, there is still some residual scatter, which is unexplained by the abundance patterns assumed here and might point to more complex abundance pattern variations between stars.

The differences in response functions for the higher-order Balmer features, from different theoretical models, lead to uncertainties in both the ages and chemistry of stars and stellar populations. This is an additional uncertainty not normally taken into account by authors who publish stellar population parameters and draw conclusions from the fitting of Lick indices. As indicated earlier, there is a move towards a generation of whole spectral SSPs and fitting of such to data, rather than using indices. This full spectrum fitting approach will also be affected by any mismatches between theoretical predictions and empirical observations. It is recommended that future generations of SSP model producers, of indices or spectra, test their results on a star-by-star basis against observations for a range of star abundance patterns (i.e. a range of [Fe/H] and [α/Fe]), in order to check for any discrepancies in the predictions, such as those found here for the higher-order Balmer features and for other features (e.g. Ca4227). It is particularly important to check against empirical measurements of indices, because these isolate the parts of the spectra that help most to break the well-known degeneracies, and to isolate features most sensitive to particular element abundances.

The spectral ratios shown in Section 4 illustrate the fact that the impact of abundance variations on the blue region of the spectrum decreases with increasing temperature. This is seen in Fig. 9 where the ratios of stars at fixed [Z/H], but varying [Fe/H] and [Mg/H], are plotted in order of increasing temperature, which show decreasing variations with increasing temperature. This result is larger than the uncertainties due to stellar parameters, assessed from studies of similar stars. Therefore, the study of abundance effects in the blue region of the spectrum is particularly important for cool stars.

6 CONCLUSIONS

The effects of element abundance changes on the strengths of spectral features in the spectra of different types of stars have been investigated. Theoretical response functions, widely used to measure abundance patterns in observed stellar populations, are tested against empirical data for stars from MILES with measured abundances of [Fe/H] and [Mg/Fe]. Using the empirical [Mg/Fe] measurements from M11 as a proxy for overall [α/Fe] values, the following results are found from these tests.

(i) For the K05 response functions, the Fe-sensitive features largely follow the observations, whereas the Hγ and Hδ features show systematically different behaviour between theoretical predictions and empirical observations. For the Hγ and Hδ features, warm stars show a wider range of indices than predicted, whereas the opposite is true for cool stars. Indices sensitive to other elements show weaker trends, with larger scatter about the one-to-one lines (e.g. Mgb and Mg_2). The calcium-sensitive feature (Ca4227) shows a negligible trend, implying that additional factors affect this index apart from overall [α/Fe].

(ii) For the H02 response functions, similar results are found as for the K05 comparisons. However, the agreement between theory and observations is improved for the Hγ and Hδ features in cool stars when the H02 response functions are used.

(iii) It is important to compile and obtain results for [Ca/Fe] measurement for MILES stars in future, to gain a better understanding of the influence of calcium on specific features, such as Ca4227. It is also important to obtain future measurements of carbon and nitrogen abundances for the stars studied in this paper from high-resolution spectra, in order to better understand the element responses of CN_1, CN_2, Ca4227 and other features.

(iv) For the W12 star response functions (used in L09), together with K05 [Z/H] overall metallicity responses, similar patterns are found. These W12 star response functions could also be used to compare many more stars in order to explore small changes in [α/Fe] only. This shows typically a large scatter between normalized observations and normalized theoretical predictions, with weak trends about the one-to-one line for Mg_2, Mgb and NaD indices.

(v) Full spectrum comparisons show that changes in the blue part of the spectrum are largely a result of changes in [Fe/H] abundance. These changes decrease with increasing star temperature.

(vi) Overall [Z/H] is not always the most appropriate way to rank stars, because abundances of individual elements have important effects on emergent spectra. In general, this is particularly important in the blue part of the spectra of cool stars, where Fe, C and N abundances strongly affect the spectral shape.

(vii) The spectral results so far indicate the need for deeper observational and theoretical studies of the blue part of stellar spectra, to search for more measurable metallicity indicators, sensitive to iron abundance and to other element abundances in different types of stars. For example, indices in the blue have been defined by Rose (1994) and Serven et al. (2005). We will explore this direction in a future paper.

In summary, in this paper, we have shown that the theoretical response functions of K05 and H02 work quite well for most Lick spectral indices, with the exception of systematic offsets in the Hγ and Hδ features, when compared to observed stars. This effect is important for individual stars and, to a lesser extent, for stellar population analysis, where the opposite systematics of warm and cool stars partially compensate for each other. The response functions need to be applied in a careful and limited way, taking into account the expected spread of values and types of indices, on an index-by-index basis. If response functions are applied automatically in a single method and for unlimited abundance variations, then they will produce spurious results in derived abundance patterns and in stellar population ages.

ACKNOWLEDGEMENTS

We thank Paula Coelho for insightful discussions and comments on the manuscript. We thank IAC and UCLan for travel funding, facilitating the work carried out for this paper. A Brazilian grant from Coordenação de Aperfeiçoamento de Pessoal de Nível Superior (CAPES) was awarded to AdCM for a visit to UCLan. We also thank the Brazilian funding organization Fundação de Amparo à Pesquisa do Estado de São Paulo (FAPESP) for travel funding support for AES (grant number 2012/04953-0). This work has been supported by the Programa Nacional de Astronomía y Astrofísica of the Spanish Ministry of Economy and Competitiveness (MINECO) under grant AYA2010-21322-C03-02. We thank G. Worthey for providing us with information and values for their star response functions, and also B. Barbuy for software used to compute overall abundances from an abundance pattern. Finally, we thank an anonymous referee, who pointed out additional aspects to be considered when presenting this work.

REFERENCES

Annibali F., Grutzbauch R., Rampazzo R., Bressan A., Zeilinger W. W., 2011, A&A, 528, 19
Bell R. A., Gustafsson B., 1989, MNRAS, 236, 653
Bell R. A., Paltoglou G., Tripicco M. J., 1994, MNRAS, 268, 771
Bensby T., Feltzing S., Lundström I., Ilyin I., 2005, A&A, 433, 185
Carter D. et al., 2009, MNRAS, 397, 695
Casagrande L., Portinari L., Flynn C., 2006, MNRAS, 373, 13 (Ce06)
Cassisi S., Salaris M., Castelli F., Pietrinferni A., 2004, ApJ, 616, 498
Cenarro A. J., Sanchez-Blazquez P., Cardiel N., Gorgas J., 2004, ApJ, 614, L101
Cenarro A. J. et al., 2007, MNRAS, 374, 664
Cenarro A. J., Cardiel N., Vazdekis A., Gorgas J., 2009, MNRAS, 396, 1895
Cervantes J. L., Vazdekis A., 2009, MNRAS, 392, 691
Clementini G., Gratton R. G., Carretta E., Sneden C., 1999, MNRAS, 302, 22
Coelho P., Barbuy B., Melendez J., Schiavon R.P, Castilho B. V., 2005, A&A, 443, 735
Coelho P., Bruzual G., Charlot S., Weiss A., Barbuy B., Ferguson J. W., 2007, MNRAS, 382, 498
Da Silva R., Milone A. C., Reddy B. E., 2011, A&A, 526, A71
Delgado Mena E., Israelian G., González Hernández J. I., Bond J. C., Santos N. C., Udry S., Mayor M., 2010, ApJ, 725, 2349 (DM10)
Ecuvillon A., Israelian G., Santos N. C., Mayor M., Villar V., Bihain G., 2004, A&A, 426, 619 (Ee04)
Ecuvillon A., Israelian G., Santos N. C., Shchukina N. G., Mayor M., Rebolo R., 2006, A&A, 445, 633 (Ee06)
Falcón-Barroso J., Sánchez-Blázquez P., Vazdekis A., Ricciardelli E., Cardiel N., Cenarro A. J., Gorgas J., Peletier R. F., 2011, A&A, 532, 95
Franchini M., Morossi C., Di Marcantonio P., Malagnini M. L., Chavez M., 2011, ApJ, 730, 117
Garcia Lopez R. J., Rebolo R., Herrero A., Beckman J. E., 1993, ApJ, 412, 173 (GL93)
Graves G. J., Schiavon R. P., 2008, ApJS, 177, 446
Grevesse N., Sauval A. J., 1998, Space Sci. Rev., 85, 161
Houdashelt M. L., Trager S. C., Worthey G., Bell R. A., 2002, BAAS, 201, 1405 (H02)
James P. A., Salaris M., Davies J. I., Phillipps S., Cassisi S., 2006, MNRAS, 367, 339
Jones L. A., 1999, PhD thesis, University of North Carolina
Kobayashi C., Umeda H., Nomoto K., Tominaga N., Ohkubo T., 2006, ApJ, 653, 1145
Korn A. J., Maraston C., Thomas D., 2005, A&A, 438, 685 (K05)
Kurucz R. L., 1970, atlas: A Computer Program for Calculating Model Stellar Atmospheres. SAO Special Report, Smithsonian Astrophysical Observatory, Cambridge, MA
Lee H-c. et al., 2009a, ApJ, 694, 902 (L09)
Lee H-c., Worthey G., Dotter A., 2009b, AJ, 138, 1442
Luck R. E., Heiter U., 2006, AJ, 131, 3069 (LH06)
Luck R. E., Heiter U., 2007, AJ, 133, 2464 (LH07)
McWilliam A., Matteucci F., Ballero S., Rich R. M., Fulbright J. P., Cescutti G., 2008, AJ, 136, 367
Mannucci F., 2008, Chin. J. Astron. Astrophys. Suppl., 8, 143
Maoz D., Sharon K., Gal-Yam A., 2010, ApJ, 722, 1879
Mendel J. T., Proctor R. N., Forbes D. A., 2007, MNRAS, 379, 1618
Milone A. de C., Sansom A. E., Sánchez-Blázquez P., 2011, MNRAS, 414, 1227 (M11)
Munari U., Sordo R., Castelli F., Zwitter T., 2005, A&A, 442, 1127
Neves V., Santos N. C., Sousa S. G., Correia A. C. M., Israelian G., 2009, A&A, 497, 563
Pancino E., Carrera R., Rossetti E., Gallart C., 2010, A&A, 511, 56
Percival S. M., Salaris M., Cassisi S., Pietrinferni A., 2009, ApJ, 690, 427
Petigura E. A., Marcy G. W., 2011, ApJ, 735, 41 (PM11)
Prochaska L. C., Rose J. A., Schiavon R. P., 2005, AJ, 130, 2666
Proctor R. N., Sansom A. E., 2002, MNRAS, 333, 517
Ramírez I., Allende Prieto C., Lambert D. L., 2007, A&A, 465, 271 (Re07)
Rose J. A., 1994, AJ, 107, 206

Sánchez-Blázquez P. et al., 2006, MNRAS, 371, 703 (SB06)
Sansom A. E., Northeast M. N., 2008, MNRAS, 387, 331
Schiavon R., 2007, ApJS, 171, 146
Serra P., Trager S. C., Oosterloo T. A., Morganti R., 2008, A&A, 483, 57
Serven J., Worthey G., Briley M. M., 2005, ApJ, 627, 754
Smith R. J., Lucey J. R., Hudson M. J., Bridges T. J., 2009, MNRAS, 398, 119
Soubiran C., Girard P., 2005, A&A, 438, 139 (SG05)
Sullivan M. et al., 2006, ApJ, 648, 868
Takeda Y., Honda S., 2005, PASJ, 57, 65
Tantalo R., Chiosi C., Piovan L., 2007, A&A, 462, 481 (T07)
Thomas D., Maraston C., Bender R., 2003, MNRAS, 339, 897
Thomas D., Johansson, Maraston C., 2011, MNRAS, 412, 2199
Timmes F. X., Woosley S. E., Weaver T. A., 1995, ApJS, 98, 617
Trager S., Worthey G., Faber S. M., Burstein D., González J. J., 1998, ApJS, 116, 1
Trager S., Faber S. M., Worthey G., González J. J., 2000, AJ, 119, 1645
Trevisan M., Barbuy B., Eriksson K., Gustafsson B., Grenon M., Pompéia L., 2011, A&A, 535, A42
Tripicco M. J., Bell R. A., 1995, ApJ, 110, 3035 (TB95)
Tsujimoto T., Nomoto K., Yoshii Y., Hashimoto M., Yanagida S., Thielemann F.-K., 1995, MNRAS, 277, 945
Vazdekis A., Peletier R. F., Beckman J. E., Casuso E., 1997, ApJS, 111, 203
Vazdekis A., Cenarro A. J., Gorgas J., Cardiel N., Peletier R. F., 2003, ApJS, 111, 203
Vazdekis A., Sánchez-Blázquez P., Falcón-Barroso J., Cenarro A. J., Beasley M. A., Cardiel N., Gorgas J., Peletier R. F., 2010, MNRAS, 404, 1639
Walcher C. J., Coelho P., Gallazzi A., Charlot S., 2009, MNRAS, 398, L44
Worthey G., 1994, AJ, 128, 2826
Worthey G., Ottaviani D. L., 1997, ApJS, 111, 377 (WO97)
Zhao G., Chen Y. Q., Qiu H. M., Li Z. W., 2002, AJ, 124, 2224 (Ze02)
Zhu G., Blanton M. R., Moustakas J., 2010, ApJ, 722, 491

APPENDIX A: PARAMETERS FOR THREE CATEGORIES OF MILES STARS

This appendix shows tables of data for seven CD, 31 TO and 13 CG stars, used in testing the K05 and H02 response functions in this

Table A1. Tables of data for stars corresponding to the base model $T_{\rm eff}$ and log g values in K05, for CD, TO and CG stars, from a 5 Gyr old population.'M' in column 7 denotes the MILES star number. All 25 Lick indices are available in the online version.

No.	Name	$T_{\rm eff}$	log g	[Fe/H]	[Mg/Fe]	M	H$\delta_{\rm A}$	H$\delta_{\rm F}$	CN$_1$	CN$_2$	Ca4227	G4300	H$\gamma_{\rm A}$	H$\gamma_{\rm F}$
CD stars. Model = ($T_{\rm eff}$ = 4575.0, log g = 4.60)														
1	HD032147	4658	4.47	0.020	−0.056	168	−7.127	−1.370	0.101	0.150	3.527	5.809	−10.765	−3.638
2	HD131977	4501	4.70	0.020	0.124	532	−6.714	−1.176	0.025	0.076	4.021	5.471	−10.360	−3.266
3	HD156026	4541	4.54	−0.370	0.157	625	−5.710	−0.976	−0.021	0.034	4.642	4.967	−9.665	−3.166
4	HD103932	4510	4.57	0.160	−0.049	426	−6.926	−1.156	0.058	0.113	4.356	5.620	−11.064	−3.831
5	BD+430699	4608	4.52	−0.600	0.237	115	−5.430	−1.000	−0.002	0.038	3.183	5.331	−8.960	−3.053
6	HD021197	4616	4.59	0.300	−0.098	117	−6.463	−1.072	0.049	0.103	4.491	5.558	−11.053	−3.551
7	HD108564	4594	4.67	−1.090	0.516	442	−3.606	−0.158	−0.016	0.026	3.105	4.949	−7.847	−2.786
TO stars. Model = ($T_{\rm eff}$ = 6200.0, log g = 4.10)														
1	BD+342476	6205	4.12	−2.050	0.187	491	4.391	3.402	−0.089	−0.057	0.110	−0.307	3.953	3.419
2	HD000400	6205	4.12	−0.330	0.106	7	2.798	2.492	−0.083	−0.057	0.480	2.991	0.674	2.028
3	HD009826	6134	4.09	0.110	0.115	63	2.318	2.270	−0.080	−0.053	0.650	3.500	−0.108	1.831
4	HD014938	6153	4.04	−0.350	0.115	86	2.573	2.427	−0.071	−0.042	0.393	2.536	0.672	2.124
5	HD016673	6253	4.28	0.050	0.045	92	2.721	2.487	−0.085	−0.055	0.597	3.067	0.614	2.076
6	HD043318	6224	3.93	−0.150	0.059	213	2.861	2.550	−0.081	−0.054	0.337	2.866	1.055	2.356
7	HD074000	6166	4.19	−2.020	0.377	310	3.832	3.165	−0.079	−0.050	0.160	−0.049	3.465	3.117
8	HD076910	6275	4.10	−0.500	0.184	328	4.087	3.201	−0.089	−0.056	0.292	1.576	2.806	3.126
9	HD084937	6228	4.01	−2.170	0.440	363	4.460	3.589	−0.091	−0.062	0.049	−0.351	4.089	3.512
10	HD089744	6219	3.95	0.230	0.009	384	2.592	2.361	−0.077	−0.049	0.628	3.356	0.207	2.071
11	HD097916	6238	4.03	−0.990	0.454	405	4.690	3.559	−0.093	−0.058	0.264	0.847	3.693	3.587
12	HD102870	6109	4.20	0.170	−0.007	422	1.924	2.074	−0.070	−0.043	0.678	3.793	−0.686	1.556
13	HD107213	6298	4.01	0.290	0.133	438	2.816	2.505	−0.082	−0.053	0.488	3.476	0.321	2.122
14	HD114642	6249	3.90	−0.180	0.080	464	3.993	3.011	−0.095	−0.063	0.433	2.310	2.170	2.999
15	HD142860	6272	4.17	−0.160	0.070	576	3.045	2.622	−0.082	−0.050	0.477	2.619	1.515	2.526
16	HD159307	6198	3.90	−0.730	0.178	635	4.082	3.125	−0.096	−0.063	0.343	1.819	2.631	3.000
17	HD173667	6280	3.97	0.050	0.046	695	3.944	3.025	−0.097	−0.062	0.449	2.253	2.471	3.110
18	HD181096	6276	4.09	−0.260	0.119	716	3.523	2.879	−0.087	−0.057	0.396	2.400	1.700	2.725
19	HD215648	6167	4.04	−0.320	0.172	843	2.769	2.396	−0.078	−0.046	0.459	3.034	0.780	2.137
20	HD219623	6155	4.17	−0.040	0.026	868	2.057	2.211	−0.076	−0.049	0.646	3.664	−0.523	1.641
21	HD222368	6170	4.09	−0.150	0.131	888	2.671	2.371	−0.083	−0.054	0.519	3.088	0.616	2.160
22	HD338529	6165	4.06	−2.250	0.253	725	4.544	3.532	−0.093	−0.056	0.096	−0.399	4.295	3.510
23	HD097855	6260	4.05	−1.030	0.003	406	3.625	3.009	−0.081	−0.050	0.391	2.007	2.032	2.812
24	HD014221	6295	3.91	−0.350	0.041	83	4.154	3.265	−0.082	−0.050	0.353	1.615	2.761	3.366
25	BD+092190	6270	4.11	−2.860	0.477	348	4.914	3.817	−0.103	−0.068	0.061	−0.825	4.827	3.853
26	HD089995	6233	3.95	−0.340	−0.046	385	3.907	3.063	−0.088	−0.056	0.306	1.741	2.485	3.064
27	HD128429	6266	4.12	−0.130	0.267	518	3.408	2.864	−0.089	−0.054	0.417	2.550	2.023	2.834
28	HD173093	6268	4.09	−0.180	0.123	692	3.504	2.872	−0.086	−0.054	0.499	2.515	1.961	2.820
29	HD209369	6288	3.90	−0.280	0.153	822	3.843	2.851	−0.090	−0.059	0.383	1.938	2.582	3.183
30	HD218804	6261	4.05	−0.230	−0.054	862	4.078	3.219	−0.093	−0.060	0.464	1.714	2.982	3.294
31	BD+592723	6112	4.17	−2.020	0.528	876	3.609	3.108	−0.073	−0.048	0.152	0.044	3.090	2.808

Table A1 – *continued*

No.	Name	$T_{\rm eff}$	log g	[Fe/H]	[Mg/Fe]	M	H$\delta_{\rm A}$	H$\delta_{\rm F}$	CN$_1$	CN$_2$	Ca4227	G4300	H$\gamma_{\rm A}$	H$\gamma_{\rm F}$
CG stars. Model = ($T_{\rm eff}$ = 4255.0, log g = 1.90)														
1	HD131430	4190	1.95	0.100	−0.398	528	−7.221	−1.969	0.291	0.341	2.315	6.386	−11.045	−3.348
2	HD075691	4270	2.12	−0.050	0.015	321	−6.601	−1.619	0.220	0.267	1.929	6.321	−9.967	−3.006
3	HD113092	4283	1.95	−0.370	0.182	457	−4.085	−0.698	0.131	0.178	1.209	7.001	−8.716	−2.690
4	HD191046	4317	2.01	−0.650	0.474	755	−3.513	−0.834	0.076	0.111	1.036	6.952	−7.594	−2.424
5	HD020893	4340	2.04	0.080	−0.102	114	−5.997	−1.414	0.248	0.295	1.889	6.310	−10.137	−3.109
6	HD066141	4258	1.90	−0.300	0.061	289	−5.395	−1.068	0.167	0.216	1.614	6.564	−9.383	−3.176
7	HD083618	4231	1.74	−0.080	−0.086	357	−6.032	−1.450	0.189	0.236	2.143	6.322	−10.357	−3.131
8	HD124186	4347	2.10	0.240	0.002	499	−7.452	−1.896	0.327	0.375	2.077	6.382	−10.773	−3.453
9	HD130705	4336	2.10	0.410	−0.029	526	−7.541	−1.875	0.373	0.423	1.968	6.467	−10.970	−3.532
10	HD136726	4159	1.91	0.130	−0.087	549	−6.397	−1.562	0.217	0.270	2.677	6.222	−10.563	−3.199
11	HD154733	4200	2.09	0.000	−0.030	620	−6.444	−1.494	0.237	0.289	2.382	6.048	−10.153	−3.235
12	HD171443	4189	1.84	−0.080	0.009	682	−6.517	−1.529	0.263	0.319	2.168	6.618	−10.300	−3.348
13	M67_F-108	4255	1.84	−0.090	0.016	919	−6.772	−1.755	0.238	0.288	2.422	6.308	−10.212	−3.253

Table B1. Polynomial fits for elements X showing how [X/Fe] varies with [Fe/H] on average, for elements modelled in the response-function tables tested. The fitted data sets are indicated in the column headed 'References', the numbers of stars fitted are shown in the column headed 'No.' and the rms deviations from the fit are shown in the final column, in dex.

Polynomial fit	[Fe/H] range	References	No.	rms
Dwarfs				
[Mg/Fe] = 0.0624+0.0110[Fe/H]+0.4672[Fe/H]^2 −0.2692[Fe/H]^3 −0.3746[Fe/H]^4	−1.2 to +0.5	SG05+LH06	818	0.096
[Ca/Fe] = 0.0254−0.1261[Fe/H]+0.0930[Fe/H]^2 −0.0024[Fe/H]^3	−1.2 to +0.5	SG05+LH06	743	0.061
[Si/Fe] = 0.0419−0.1240[Fe/H]+0.1409[Fe/H]^2 +0.0073[Fe/H]^3	−1.2 to +0.5	SG05+LH06	842	0.068
[Ti/Fe] = 0.0412−0.0649[Fe/H]+0.3384[Fe/H]^2 +0.2060[Fe/H]^3	−1.2 to +0.5	SG05+LH06	731	0.088
[Na/Fe] = 0.0233+0.0757[Fe/H]+0.5329[Fe/H]^2 +0.4258[Fe/H]^3	−1.2 to +0.3	SG05	567	0.080
[O/Fe] = 0.1004−0.7273[Fe/H]−1.1294[Fe/H]^2 −0.5616[Fe/H]^3	−1.2 to +0.3	SG05	415	0.125
Giants				
[Mg/Fe] = 0.0859+0.0361[Fe/H]+0.8155[Fe/H]^2 +0.0894[Fe/H]^3	−0.6 to +0.35	LH07	298	0.103
[Ca/Fe] = −0.0533−0.2468[Fe/H]−0.3619[Fe/H]^2 −0.7604[Fe/H]^3	−0.6 to +0.35	LH07	294	0.080
[Si/Fe] = 0.1365+0.0557[Fe/H]+0.6138[Fe/H]^2 −0.2128[Fe/H]^3 −0.6167[Fe/H]^4	−0.6 to +0.35	LH07	291	0.064
[Na/Fe] = 0.1283+0.1647[Fe/H]+0.4075[Fe/H]^2 +0.0971[Fe/H]^3	−0.6 to +0.35	LH07	298	0.076
[O/Fe] = 0.0477−0.4119[Fe/H]+1.1975[Fe/H]^2 +0.8401[Fe/H]^3	−0.6 to +0.35	LH07	298	0.110
[N/Fe] = 0.2060+0.1476[Fe/H]+0.0026[Fe/H]^2 −0.1319[Fe/H]^3	−0.6 to +0.35	LH07	298	0.100
[C/Fe] = −0.1568−0.2862[Fe/H]+1.0187[Fe/H]^2 +2.2720[Fe/H]^3 +1.7822[Fe/H]^4	−0.6 to +0.35	LH07	298	0.103

paper, and plotted in Figs 1 and 2. Details of these measurements are given Section 2.3. The [Mg/Fe] ratios are from M11. All 25 Lick indices are available in the online version.

APPENDIX B: TESTS WITH DIFFERENT ABUNDANCE RATIO TRENDS

For the results obtained in the main body of the paper, we made the assumptions that all α-element to iron ratios [α/Fe] track the value of [Mg/Fe] and that carbon and nitrogen track iron. In this appendix, we test these approximations using published data for samples of dwarf and giant stars. We fit mean trends to these data, to work out how element X varies with Mg or Fe, as a function of [Fe/H]. Table B1 shows these fits, ranges and references. Fig. B1 shows these mean relations in graphical form. The data from which these relations were obtained are plotted in published papers (SG05; LH06; LH07). These consist of at least 415 dwarf stars from SG05 (see their table 3), 216 dwarf star from LH06 (see their tables 2 and 3) and ∼298 giant stars from LH07 (see their tables 4, 5 and 7).

The enhancements of α elements (O, Ca, Si and Ti) assumed in the main body of the paper are modified by trends for [X/Mg], derived from combining [X/Mg] = [X/Fe]−[Mg/Fe] (from Table B1). Sodium is similarly modified by [Na/Mg] = [Na/Fe]−[Mg/Fe].

Table B2. Balmer line spectral index responses (changes in Å) to overall metallicity changes (by a factor of 2). Taken from tables 12 and 14 in K05 and the corresponding tables in H02.

		K05 [Z/H]	H02 [Z/H]
CD	H$\delta_{\rm A}$	−1.089	−0.704
	H$\delta_{\rm F}$	−0.546	−0.280
	H$\gamma_{\rm A}$	−1.381	−0.432
	H$\gamma_{\rm F}$	−0.269	−0.099
CG	H$\delta_{\rm A}$	−1.533	−2.112
	H$\delta_{\rm F}$	−1.252	−0.640
	H$\gamma_{\rm A}$	−1.820	−0.720
	H$\gamma_{\rm F}$	−0.534	−0.132

Nitrogen is treated as enhanced for giants, in this appendix, and scaled-solar for dwarfs (e.g. Takeda & Honda 2005). Carbon was originally assumed to follow iron in Section 3.1.1, which might be a good approximation for dwarfs (e.g. Takeda & Honda 2005; Da Silva, Milone & Reddy 2011) but not for giants (LH07). Therefore, we modify our assumed carbon abundances for giants by adding [C/Fe] (from Table B1) to our original assumption.

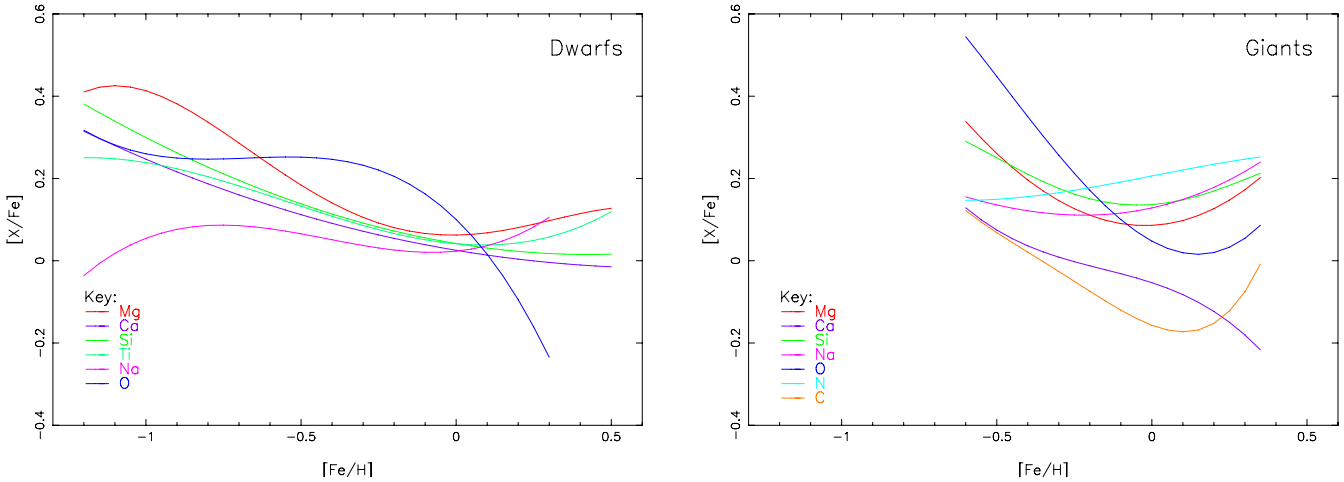

Figure B1. Mean polynomial fits for element abundance ratios [X/Fe] in dwarf stars (left plot) and giants stars (right plot) locally in the disc of the Milky Way. The horizontal ranges plotted illustrate ranges covered by the data (SG05+LH06 for dwarfs and LH07 for giants).

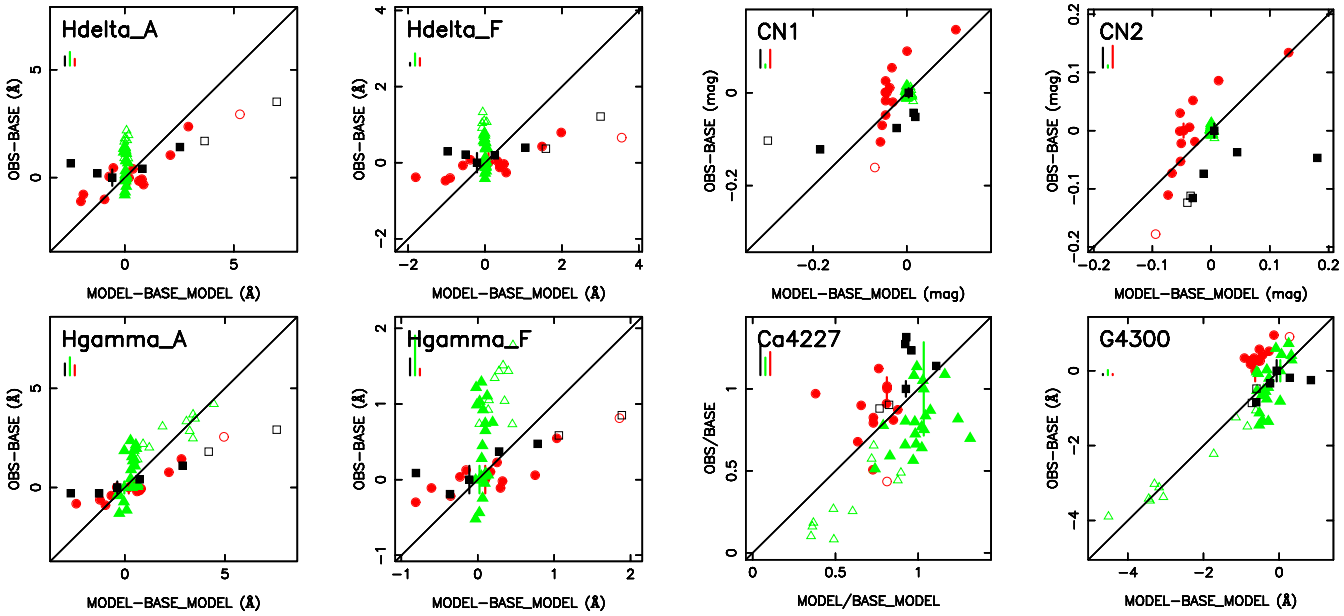

Figure B2. Testing the response functions of K05 by applying mean trends of element abundance ratios. The assumed element abundance ratios are modified by relations seen for stars in the local disc of the Milky Way. Comparison of normalized empirical versus normalized theoretical line strengths for standard Lick indices sensitive to four H Balmer lines and to four CN-sensitive indices, in the stellar photospheres. Symbols as in Fig. 1(a), with cool dwarfs (CD, black squares), turn-off stars (TO, green triangles) and cool giants (CG, red circles).

In this way, our measured [Mg/Fe] or [Fe/H] values for each star are then scaled by the above observed mean trends to generate estimates for other elements [X/Fe]. Applying these modified abundance patterns leads to similar relations, as seen in Figs 1 and 2, with the main exceptions being cool stars in the CN_1 and CN_2 bands, Ca4227 (affected by CN bands on one side), G4300 and, to a lesser extent, $C_2$4668. Tests of response functions for these features are therefore less certain, because of the greater impact of unknown C and N abundances. More robust tests of the responses for these five indices, in the blue part of the spectrum for cool stars, must await individual C and N element abundance measurements in those stars. The main results, regarding responses for iron features, Balmer features, magnesium and sodium features, remain intact. In contrast Fig. B2, which shows the Hγ and Hδ indices plus the four most uncertain features, with the same indices plotted in Fig. 1(b) and Figs 1(d) and 1(e), respectively.

For Hγ and Hδ indices, the robustness of our findings against uncertainties in individual element abundances points to the overall metallicity response as the cause of the observed difference between models and observations in Fig. 1(b). We test this here. The good agreement of iron-sensitive indices and others, such as Ca4455, indicates that the spectral responses to overall metallicity ([Z/H]) in K05 and H02 are not significantly in error for those indices, in contrast to the case for the Hγ and Hδ indices. Table B2 compares the overall metallicity responses for these four Balmer indices, from K05 and H02. From this table, we see that the spectral responses are smaller in H02 than in K05 (except for $H\delta_A$). For $H\delta_A$, the overall metallicity response is larger in H02 and this gives a worse fit to

the observations (see Table 4). For the other three Balmer indices in Table B2, the smaller values of overall metallicity response in H02 lead to an improvement in the predictions for $H\gamma_A$, $H\gamma_F$ and $H\delta_F$ indices.

SUPPORTING INFORMATION

Additional Supporting Information may be found in the online version of this article:

Table A1. Tables of data for stars corresponding to the base model $T_{\rm eff}$ and $\log g$ values in K05, for CD, TO and CG stars, from a 5-Gyr-old population. The 'M' in column 7 denotes the MILES star number (http://mnras.oxfordjournals.org/lookup/suppl/doi:10.1093/mnras/stt1283/-/DC1).

Please note: Oxford University Press are not responsible for the content or functionality of any supporting materials supplied by the authors. Any queries (other than missing material) should be directed to the corresponding author for the article.

This paper has been typeset from a TEX/LATEX file prepared by the author.